J. Fluid Mech. (2003), *vol.* 493, *pp.* 287–318.
DOI: 10.1017/S0022112003006025 Printed in the United Kingdom

The three-dimensional instability of a strained vortex tube revisited

By YASUHIDE FUKUMOTO

Graduate School of Mathematics and Space Environment Research Centre, Kyushu University 33, Fukuoka 812–8581, Japan

(Received 10 April 2002 and in revised form 10 June 2003)

We revisit the Moore–Saffman–Tsai–Widnall instability, a parametric resonance between left- and right-handed bending waves of infinitesimal amplitude, on the Rankine vortex strained by a weak pure shear flow. The results of Tsai & Widnall (1976) and Eloy & Le Dizès (2001), as generalized to all pairs of Kelvin waves whose azimuthal wavenumbers m are separated by 2, are simplified by providing an explicit solution of the linearized Euler equations for the disturbance flow field. Given the wavenumber k_0 and the frequency ω_0 of an intersection point of dispersion curves, the growth rate is expressible solely in terms of the modified Bessel functions, and so is the unstable wavenumber range. Every intersection leads to instability. Most of the intersections correspond to weak instability that vanishes in the short-wave limit, and dominant modes are restricted to particular intersections. For helical waves $m = \pm 1$, the growth rate of non-rotating waves is far larger than that of rotating waves. The wavenumber width of stationary instability bands broadens linearly in k_0, while that of rotating instability bands is bounded. The growth rate of the stationary instability takes, in the long-wavelength limit, the value of $\varepsilon/2$ for the two-dimensional displacement instability, and, in the short-wavelength limit, the value of $9\varepsilon/16$ for the elliptical instability, being larger at large but finite values of k_0. Here ε is the strength of shear near the core centre. For resonance between higher azimuthal wavenumbers m and $m + 2$, the same limiting value is approached as $k_0 \to \infty$, along sequences of specific crossing points whose frequency rapidly converges to $m + 1$, in two ways, from above for a fixed m and from below for $m \to \infty$. The energy of the Kelvin waves is calculated by invoking Cairns' formula. The instability result is compatible with Krein's theory for Hamiltonian spectra.

1. Introduction

Moore & Saffman (1975) and Tsai & Widnall (1976), hereinafter referred to as MS75 and TW76 respectively, addressed a three-dimensional linear stability problem of a straight vortex tube embedded in a plane pure shear flow with its principal axes perpendicular to the tube axis. They uncovered the essence of a parametric resonance between left- and right-handed helical waves driven by the imposed shear.

Inspired by Pierrehumbert's numerical simulation (Pierrehumbert 1986), Bayly (1986) put forward the concept of the *elliptical instability*. Flows linear in coordinates with elliptical streamlines are unstable to three-dimensional disturbances. This is extended, in a framework of geometric optics approach, to a local instability of general strained circulatory flows by Friedlander & Vishik (1991) and Lifschitz & Hameiri (1991), establishing the ubiquity of the elliptical instability. Owing to continual study

of stability of elliptical streamlines in both open and confined geometries, it is now established that the Moore–Saffman–Tsai–Widnall instability is none other than the elliptical instability except for long wavelengths for which the stability characteristics are sensitive to boundary conditions (Gledzer *et al.* 1975; Vladimirov, Tarasov & Rybak 1983; Saffman 1988; Waleffe 1990; Gledzer & Ponomarev 1992; Miyazaki, Imai & Fukumoto 1995; Leweke & Williamson 1998; Eloy & Le Dizès 2001; Kerswell 2002). Yet, an easier route that links the global to the local stability will, if available, be helpful.

The assumption of *constant* vorticity in the core, taken by TW76, is advantageous in that the linear stability is analytically tractable to a great extent. However, unimplemented integrals are left in their expressions for disturbance flow field and thence the instability characteristics. These integrals appear to hinder full mathematical and numerical analyses, and to mask their physical implications.

In the present investigation, we make an attempt at simplifying the results of TW76. The problem is the weak-shear limit of the three-dimensional linear stability of the Moore–Saffman elliptic vortex (Moore & Saffman 1971) investigated numerically by Robinson & Saffman (1984). We show that the Euler equations for the disturbance flow field are solvable, to first order in the shear strength ε, solely in terms of the Bessel and the modified Bessel functions, without having to include integrals. In general, the elliptic vortex goes through a parametric resonance when two Kelvin waves whose azimuthal wavenumbers m differ by 2 are simultaneously excited as investigated by Gledzer & Ponomarev (1992) through the Galerkin method and by Eloy & Le Dizès (2001, hereinafter referred to as EL01), through the Moore–Saffman approach. Eloy, Le Gal & Le Dizès (2000) observed $(m, m+2) = (1, 3)$ and $(0, 2)$ resonance for a flow in an elliptical cylinder of finite extent, depending on the Reynolds number and the cylinder length (see figure 4 of Kerswell 2002). This paper covers all combinations of azimuthal wavenumbers m and $m+2$. Compact formulae are presented not only for the growth rate and the wavenumber range of unstable modes, but for the corresponding eigenfunctions.

These formulae will reveal the mathematical structure behind the predominance of the stationary mode, the one with frequency $\omega_0 = 0$, for bending waves, and generally with $\omega_0 \approx m+1$ for $(m, m+2)$ resonance. EL01 clarified that only these modes survive in the short-wave limit, with the maximum growth rate being $9\varepsilon/16$, the value derived by Waleffe (1990). The others are very weak and vanish in the short-wave limit. The closed form of solution is amenable to higher-order asymptotic expansions. The augmented terms in the short-wave asymptotics will tell that the growth rate overshoots $9\varepsilon/16$ at large values of k_0 in this open flow, contrary to the cases of confined flows. Also shown is the widening, linear in k_0, of the wavenumber width of the instability band, being reflective of the broadband nature of the elliptical instability.

A clue to the understanding of the wavenumber dependence of spectra lies in Krein's theory of parametric resonance in Hamiltonian systems (Krein 1950; MacKay 1986; Saffman 1992). A single Kelvin wave cannot be fed by a perturbation breaking the circular symmetry. The pure shear, a quadrupole field, plays the role of perturbation. Subject to it, two Kelvin waves with their azimuthal wavenumber difference being 2 can be cooperatively amplifiable when the eigenvalues $-\mathrm{i}\omega_0$ collide on the imaginary axis as the parameter k_0 is varied, provided either that the collision frequency is zero or that the signs of the wave energy are different from each other at a non-zero frequency. Since the wave energy is quadratic in amplitude, nonlinear solution of waves on the Rankine vortex would be required. Cairns' formula (Cairns 1979; Craik

1985) offers an efficient machinery to bypass this procedure. An effort is made to put our result on Krein's scenario.

In § 2, we give a statement of the problem. The Kelvin waves are recalled in § 3. Section 4 accommodates the linearized Euler equations to examine how the quadrupole field affects, to $O(\varepsilon)$, the Kelvin waves. In § 5, the equations are integrated for helical waves $m = \pm 1$. The eigenvalue problem to $O(\varepsilon)$ encounters a singularity at $\omega_0 = 0$. Care is exercised for the stationary waves in § 5.1, which precedes the case of $\omega_0 \neq 0$ in § 5.2. In addition to carrying through the numerical calculation, both long- and short-wave asymptotics are derived. Section 6, supplemented by Appendices A and B, is concerned with resonance between general azimuthal wavenumbers m and $m + 2$. In § 7, the excess energy necessary to excite the Kelvin waves is calculated through Cairns' formula. A direct derivation of energy is made for two-dimensional waves in Appendix C, which serves as a self-consistency justification to this formula. The last section (§ 8) is devoted to a summary and conclusions.

2. Setting of the stability problem

The basic flow is a steady perturbation solution of the Euler equations for a columnar vortex of uniform vorticity subject to a plane pure shear with its principal axes orthogonal to vorticity. The shear strength ε is assumed to be small: $\varepsilon \ll 1$. The notation follows that of TW76.

In the absence of shear, the basic flow is a straight vortex tube with circular core of radius a and circulation Γ, surrounded by an irrotational flow of infinite expanse. Let us introduce cylindrical coordinates (r, θ, z) with the z-axis along the centreline of the core. The radial coordinate r is normalized by a, the velocity by the maximum azimuthal velocity $\Gamma/2\pi a$, and the pressure by $\rho(\Gamma/2\pi a)^2$ with ρ being the density of fluid. Let the r- and θ-components of velocity field be U and V, and the pressure be P. We denote by Φ the velocity potential for the irrotational flow field outside the core. The exact solution for the Moore–Saffman elliptic vortex is expanded, to $O(\varepsilon)$, as

$$\left.\begin{aligned} &U = \varepsilon U_1(r,\theta) + \cdots, \quad V = V_0(r) + \varepsilon V_1(r,\theta) + \cdots, \\ &P = P_0(r) + \varepsilon P_1(r,\theta) + \cdots, \quad \Phi = \Phi_0(\theta) + \varepsilon \Phi_1(r,\theta) + \cdots. \end{aligned}\right\} \tag{2.1}$$

The subscript designates order in ε. The leading-order flow is the Rankine vortex:

$$V_0 = \begin{cases} r, & \\ \dfrac{1}{r}, & \end{cases} \qquad P_0 = \begin{cases} \frac{1}{2}r^2 - 1 & (r \leqslant 1), \\ -\dfrac{1}{2r^2} & (r > 1). \end{cases} \tag{2.2}$$

The first-order perturbation is a pure shear flow, or a quadrupole field, as given by

$$\left.\begin{aligned} &U_1 = -r\sin 2\theta, \quad V_1 = -r\cos 2\theta, \quad P_1 = 0 \quad \text{for} \quad r \leqslant R(\theta,\varepsilon), \\ &\Phi_1 = \frac{1}{4}\left(\frac{1}{r^2} - r^2\right)\sin 2\theta \quad \text{for} \quad r > R(\theta,\varepsilon). \end{aligned}\right\} \tag{2.3}$$

The boundary shape $r = R(\theta, \varepsilon)$ of core cross-section is an ellipse of small eccentricity with the major axis along the x-axis ($\theta = 0$):

$$R(\theta,\varepsilon) = 1 + \tfrac{1}{2}\varepsilon\cos 2\theta + O(\varepsilon^2). \tag{2.4}$$

It deserves mention that the $O(\varepsilon)$ shear varies with distance from vortex centre. In Cartesian coordinates (x, y) in the transversal plane, (2.3) looks like

$$\begin{aligned} \varepsilon \boldsymbol{V}_1 &= (-\varepsilon y, -\varepsilon x) \quad \text{for} \quad r < R(\theta, \varepsilon), \\ &\approx \left(-\tfrac{1}{2}\varepsilon y, -\tfrac{1}{2}\varepsilon x\right) \quad \text{as} \quad r \to \infty. \end{aligned} \tag{2.5}$$

The shear strength at large distances is half as large as the local one near $r = 0$.

We inquire into evolution of three-dimensional disturbances of infinitesimal amplitude superposed on this steady strained vortex. Suppose that the boundary of the core is disturbed to

$$r = R(\theta, \varepsilon) + \eta(\theta, z, t, \varepsilon), \tag{2.6}$$

where we may assume superposition of normal modes for the disturbance amplitude η. Following the prescription of MS75 and TW76, we seek the solution for the disturbance velocity $\tilde{\boldsymbol{v}}$, the disturbance pressure $\tilde{p}$ and the external disturbance velocity-potential $\tilde{\phi}$ in a power series of ε to first order:

$$\left.\begin{aligned} &\tilde{\boldsymbol{v}} = \mathrm{Re}\left[(\boldsymbol{v}_0 + \varepsilon \boldsymbol{v}_1 + \cdots)\mathrm{e}^{\mathrm{i}(kz-\omega t)}\right], \quad \tilde{p} = \mathrm{Re}\left[(\pi_0 + \varepsilon \pi_1 + \cdots)\mathrm{e}^{\mathrm{i}(kz-\omega t)}\right], \\ &\tilde{\phi} = \mathrm{Re}\left[(\phi_0 + \varepsilon \phi_1 + \cdots)\mathrm{e}^{\mathrm{i}(kz-\omega t)}\right]. \end{aligned}\right\} \tag{2.7}$$

Concomitantly, wavenumber k and frequency ω are also expanded in powers of ε as

$$k = k_0 + \varepsilon k_1 + \cdots, \quad \omega = \omega_0 + \varepsilon \omega_1 + \cdots. \tag{2.8}$$

We are concerned only with the real part of the complex disturbance field, though the symbol Re is dropped in the rest of paper. The spectrum is unchanged for $k_0 \to -k_0$, and therefore we limit our attention to $k_0 \geqslant 0$.

3. Kelvin waves

For an introduction of notations and for later use, we are reminded of the dispersion relation and the velocity field of the Kelvin waves, before entering into the straining effect. The detail is found, for example, in TW76, Kopiev & Chernyshev (1997) and Saffman (1992).

Suppose that an infinitesimal-amplitude wave is superposed on the Rankine vortex, by deforming the circular core into

$$r = \eta(\theta, z, t) = 1 + A_0^{(m)} \exp[\mathrm{i}(m\theta + k_0 z - \omega_0 t)]. \tag{3.1}$$

As a consequence, the disturbance flow field (2.7) takes, to $O(\varepsilon^0)$, the following form:

$$\boldsymbol{v}_0 = \boldsymbol{v}_0^{(m)}(r)\mathrm{e}^{\mathrm{i}m\theta}, \quad \pi_0 = \pi_0^{(m)}(r)\mathrm{e}^{\mathrm{i}m\theta}, \quad \phi_0 = \phi_0^{(m)}(r)\mathrm{e}^{\mathrm{i}m\theta}. \tag{3.2}$$

We define

$$\eta_m^2 = \left[4/(\omega_0 - m)^2 - 1\right] k_0^2, \tag{3.3}$$

and denote the z-component of disturbance velocity by w. A general solution of the linearized Euler equations is

$$\phi_0^{(m)} = K_m(k_0 r)\alpha_0^{(m)} \quad \text{for} \quad r > \eta, \tag{3.4}$$

and

$$\left.\begin{aligned}
\pi_0^{(m)} &= J_m(\eta_m r)\beta_0^{(m)},\\
u_0^{(m)} &= \frac{\mathrm{i}}{\omega_0 - m + 2}\left\{-\frac{m}{r}J_m(\eta_m r) + \frac{\omega_0 - m}{\omega_0 - m - 2}\eta_m J_{m+1}(\eta_m r)\right\}\beta_0^{(m)},\\
v_0^{(m)} &= \frac{1}{\omega_0 - m + 2}\left\{\frac{m}{r}J_m(\eta_m r) + \frac{2}{\omega_0 - m - 2}\eta_m J_{m+1}(\eta_m r)\right\}\beta_0^{(m)},\\
w_0^{(m)} &= \frac{k_0}{\omega_0 - m}J_m(\eta_m r)\beta_0^{(m)} \quad \text{for} \quad r < \eta.
\end{aligned}\right\} \tag{3.5}$$

Here J_m and K_m are, respectively, the Bessel function of the first kind and the modified Bessel function of the second kind, m being their order. It should be kept in view that we have assumed

$$\omega_0 \neq m, \quad \omega_0 \neq m \pm 2. \tag{3.6}$$

The boundary conditions supply the relation that holds between the constants $\alpha_0^{(m)}$ and $\beta_0^{(m)}$ as

$$\alpha_0^{(m)} = -\frac{\mathrm{i}J_m(\eta_m)}{(\omega_0 - m)K_m(k_0)}\beta_0^{(m)}, \tag{3.7}$$

and the dispersion relation:

$$J_{m+1}(\eta_m) = \left\{\frac{2m}{\omega_0 - m + 2} - \frac{k_0 K_{m+1}(k_0)}{K_m(k_0)}\right\}\frac{\eta_m}{k_0^2}J_m(\eta_m). \tag{3.8}$$

The disturbance amplitude $A_0^{(m)}$ of the boundary shape is related to $\beta_0^{(m)}$ through

$$A_0^{(m)} = \frac{1}{4 - (\omega_0 - m)^2}\left\{-\eta_m J_{|m|-1}(\eta_m) + \frac{|m|}{\omega_0 - m}\left(\omega_0 - m + \frac{2m}{|m|}\right)J_{|m|}(\eta_m)\right\}\beta_0^{(m)}. \tag{3.9}$$

Figure 1 displays the dispersion relation (3.8) of bending waves $m = \pm 1$. Curves for $m = 1$ are drawn with solid lines, while those for $m = -1$ are drawn with dashed lines. The curves starting from $(k_0, \omega_0) = (0, 0)$, being drawn with thick lines, are isolated from other branches and are named the *isolated modes*. Its eigenfunction has a simple radial structure. Infinitely many branches emanate from $(k_0, \omega_0) = (0, 1)$ for $m = 1$ and from $(k_0, \omega_0) = (0, -1)$ for $m = -1$, among which twenty branches for each, ten upward and ten downward, are displayed. The corresponding eigenfunctions have non-trivial radial structures, and we call these the *higher radial modes* or simply the *radial modes*. A wave with $|\omega_0| > 1$ rotates faster than the basic circulatory flow and are called a *cograde* mode, which is distinguished from a wave with $|\omega_0| < 1$, a *retrograde* mode (Saffman 1992).

4. Effect of pure shear: the equations for disturbances

We explore how the pure shear (2.3) of $O(\varepsilon)$ modifies Kelvin's dispersion relation. The formulation of TW76, as generalized to $(m, m + 2)$ resonance, is delineated.

Given two Kelvin waves to $O(\varepsilon^0)$ whose wavenumbers are separated by 2,

$$\boldsymbol{v}_0 = \boldsymbol{v}_0^{(m)}\mathrm{e}^{\mathrm{i}m\theta} + \boldsymbol{v}_0^{(m+2)}\mathrm{e}^{\mathrm{i}(m+2)\theta}, \tag{4.1}$$

then the wave excited to $O(\varepsilon)$ possesses the following angular dependence:

$$\boldsymbol{v}_1 = \boldsymbol{v}_1^{(m)}\mathrm{e}^{\mathrm{i}m\theta} + \boldsymbol{v}_1^{(m+2)}\mathrm{e}^{\mathrm{i}(m+2)\theta} + \boldsymbol{v}_1^{(m-2)}\mathrm{e}^{\mathrm{i}(m-2)\theta} + \boldsymbol{v}_1^{(m+4)}\mathrm{e}^{\mathrm{i}(m+4)\theta}. \tag{4.2}$$

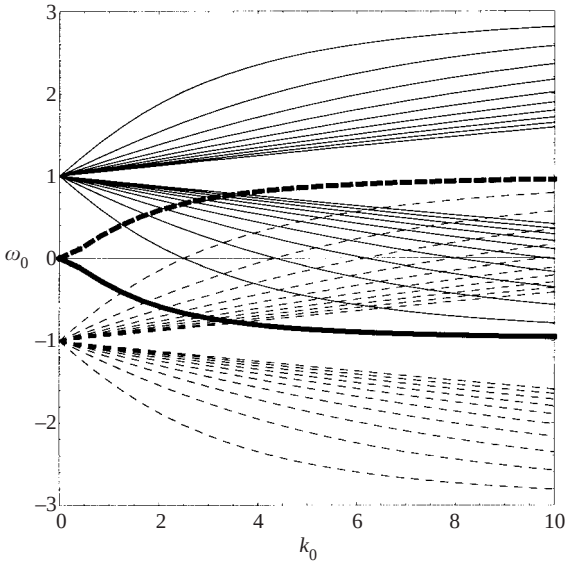

FIGURE 1. Dispersion relation of the left-handed helical wave $m = 1$ (solid lines) and the right-handed helical wave $m = -1$ (dashed lines) on the Rankine vortex. The isolated branches are shown with thick lines.

The similar form is posed on π_0, ϕ_0 and π_1, ϕ_1. The disturbance field $\boldsymbol{v}_1, \pi_1$ in the core ($r < \eta$) and the velocity potential ϕ_1 for irrotational disturbance in the ambient region ($r > \eta$), of infinitesimal amplitude, obeys

$$\left.\begin{aligned} &-\mathrm{i}\omega_0\boldsymbol{v}_1 + (\boldsymbol{V}_0\cdot\nabla_\perp)\boldsymbol{v}_1 + (\boldsymbol{v}_1\cdot\nabla_\perp)\boldsymbol{V}_0 + \nabla_\perp\pi_1 + \mathrm{i}k_0\pi_1\boldsymbol{e}_z \\ &\quad = \mathrm{i}\omega_1\boldsymbol{v}_0 - (\boldsymbol{V}_1\cdot\nabla_\perp)\boldsymbol{v}_0 - (\boldsymbol{v}_0\cdot\nabla_\perp)\boldsymbol{V}_1 - \mathrm{i}k_1\pi_0\boldsymbol{e}_z, \\ &\nabla_\perp\cdot\boldsymbol{v}_1 + \mathrm{i}k_0 w_1 = -\mathrm{i}k_1 w_0, \quad \left[\nabla_\perp^2 - k_0^2\right]\phi_1 = 2k_0k_1\phi_0, \end{aligned}\right\} \tag{4.3}$$

where $\nabla_\perp = (\partial/\partial r, 1/r\,\partial/\partial\theta)$ and $\boldsymbol{e}_z$ is the unit vector in the z-direction.

The velocity potential for the m and $m+2$ waves, finite at infinity, is readily obtainable, upon substitution from (3.4), as

$$\left.\begin{aligned} \phi_1^{(m)} &= K_m(k_0r)\alpha_1^{(m)} - k_1 r K_{m+1}(k_0r)\alpha_0^{(m)}, \\ \phi_1^{(m+2)} &= K_{m+2}(k_0r)\alpha_1^{(m+2)} - k_1 r K_{m+1}(k_0r)\alpha_0^{(m+2)}, \end{aligned}\right\} \tag{4.4}$$

where $\alpha_1^{(m)}$ and $\alpha_1^{(m+2)}$ are constants imparted to the homogeneous parts of solution.

The vortical disturbance in the core is sought by reducing, at the outset, the coupled system (4.3) of equations to a second-order ordinary differential equation for the disturbance pressure $\pi_1^{(m)}$ are $\pi_1^{(m+2)}$ in the following way:

$$\begin{aligned} L^{(m)}\pi_1^{(m)} = &\left\{\frac{8k_0^2\omega_1}{(\omega_0-m)^3} - \frac{2k_1}{k_0}\eta_m^2\right\}J_m(\eta_m r)\beta_0^{(m)} - k_0^2\left\{\frac{\omega_0-m-4}{(\omega_0-m-2)^2}J_m(\eta_{m+2}r)\right. \\ &\left. + \left[\frac{1}{(\omega_0-m)^2} - \frac{1}{(\omega_0-m-2)^2}\right]\eta_{m+2}r\,J_{m+1}(\eta_{m+2}r)\right\}\beta_0^{(m+2)}, \end{aligned} \tag{4.5}$$

$$L^{(m+2)}\pi_1^{(m+2)} = \left\{\frac{8k_0^2\omega_1}{(\omega_0-m-2)^3} - \frac{2k_1}{k_0}\eta_{m+2}^2\right\}J_{m+2}(\eta_{m+2}r)\beta_0^{(m+2)} + k_0^2\left\{\left[\frac{1}{(\omega_0-m-2)^2} - \frac{1}{(\omega_0-m)^2}\right]\eta_m r J_{m+1}(\eta_m r) + \frac{\omega_0-m+2}{(\omega_0-m)^2}J_{m+2}(\eta_m r)\right\}\beta_0^{(m)}, \tag{4.6}$$

where

$$L^{(m)} = \frac{\mathrm{d}^2}{\mathrm{d}r^2} + \frac{1}{r}\frac{\mathrm{d}}{\mathrm{d}r} - \frac{m^2}{r^2} + \eta_m^2. \tag{4.7}$$

The boundary conditions to be imposed at the core interface ($r=1$) are the kinematical and dynamical boundary conditions. They read, for the m wave,

$$\left.\begin{aligned}&\frac{\mathrm{d}\phi_1^{(m)}}{\mathrm{d}r} - u_1^{(m)} = \frac{1}{4}\frac{\mathrm{d}u_0^{(m+2)}}{\mathrm{d}r} + \frac{\mathrm{i}}{2}v_0^{(m+2)} - \frac{1}{4}\frac{\mathrm{d}^2\phi_0^{(m+2)}}{\mathrm{d}r^2} + \frac{m+2}{2}\phi_0^{(m+2)},\\ &\pi_1^{(m)} - \mathrm{i}(\omega_0-m)\phi_1^{(m)} = \mathrm{i}\omega_1\phi_0^{(m)} + \frac{\mathrm{i}(m+2)}{2}\phi_0^{(m+2)} + \frac{\mathrm{i}(\omega_0-m)}{4}\frac{\mathrm{d}\phi_0^{(m+2)}}{\mathrm{d}r} - \frac{1}{4}\frac{\mathrm{d}\pi_0^{(m+2)}}{\mathrm{d}r},\end{aligned}\right\} \tag{4.8}$$

and, for the $m+2$ wave,

$$\left.\begin{aligned}&\frac{\mathrm{d}\phi_1^{(m+2)}}{\mathrm{d}r} - u_1^{(m+2)} = \frac{1}{4}\frac{\mathrm{d}u_0^{(m)}}{\mathrm{d}r} - \frac{\mathrm{i}}{2}v_0^{(m)} - \frac{1}{4}\frac{\mathrm{d}^2\phi_0^{(m)}}{\mathrm{d}r^2} - \frac{m}{2}\phi_0^{(m)},\\ &\pi_1^{(m+2)} - \mathrm{i}(\omega_0-m-2)\phi_1^{(m+2)} = \mathrm{i}\omega_1\phi_0^{(m+2)} + \frac{\mathrm{i}m}{2}\phi_0^{(m)} + \frac{\mathrm{i}(\omega_0-m-2)}{4}\frac{\mathrm{d}\phi_0^{(m)}}{\mathrm{d}r} - \frac{1}{4}\frac{\mathrm{d}\pi_0^{(m)}}{\mathrm{d}r}.\end{aligned}\right\} \tag{4.9}$$

So far we have, though generalized, kept track of the formulation of TW76. We are now in a position to show that (4.5) and (4.6) are explicitly solvable in a compact form. We begin with the case of $m=-1$, namely the helical–helical wave resonance, in § 5 and then a general case of $m \geqslant 0$ follows in § 6.

5. Resonance between the helical waves $m = \pm 1$

An intuitive argument, by Widnall, Bliss & Tsai (1974) and Moore & Saffman (1975), that the self-induced rotation of a sinusoidally deformed vortex filament has a stabilizing effect led us to a belief that the most unstable mode is stationary. In light of this, bending waves have attracted most of our attention. It turns out that the solution entails a singularity at $\omega_0 = 0$ (see (A 1)), which calls for an individual treatment. First we describe the stationary mode in § 5.1, and thereafter turn to the case of $\omega_0 \neq 0$ in § 5.2. We use super and subscripts $+$ and $-$ in place of $m=+1$ and $m=-1$, respectively.

5.1. *The case of* $\omega_0 = 0$

When restricted to $\omega_0 = 0$, (3.3) becomes

$$\eta_+ = \eta_- = \sqrt{3}k_0. \tag{5.1}$$

To obtain $\pi_1^{(+)}$, it suffices to make a change $\beta_0^{(\pm)} \to -\beta_0^{(\pm)}$ and $\omega_1 \to -\omega_1$ in $\pi_1^{(-)}$. Inspection brings us a general solution for $\pi_1^{(-)}$, finite at $r=0$, of (4.5) with $\omega_0 = 0$

and $m=-1$ in closed form. Gathering together, they are written as

$$\pi_1^{(\pm)} = \pm J_1(\sqrt{3}k_0 r)\beta_1^{(\pm)} + \left\{ \frac{4\omega_1}{\sqrt{3}} k_0 \pm \sqrt{3}k_1 \right\} r J_0(\sqrt{3}k_0 r)\beta_0^{(\pm)} \mp \frac{\sqrt{3}}{2} k_0 r J_0(\sqrt{3}k_0 r)\beta_0^{(\mp)}. \tag{5.2}$$

Here, $\beta_1^{(\pm)}$ is a constant associated with the homogeneous solution and we have made use of $J_{-1}(x)=-J_1(x)$ and $K_{-1}(x) = K_1(x)$. Notice that (5.2) is free from integrals of multiples of the Bessel functions. Once the disturbance pressure is available, the disturbance velocity field in the core is deduced immediately by returning to the Euler equations (4.3) as follows:

$$\begin{aligned} u_1^{(\pm)} = -\frac{\mathrm{i}}{3}\Bigg\{ & \sqrt{3}k_0 J_0(\sqrt{3}k_0 r) + \frac{J_1(\sqrt{3}k_0 r)}{r} \Bigg\}\beta_1^{(\pm)} \\ & + \mathrm{i}\Bigg\{ \pm\omega_1 \Bigg[-\frac{7k_0}{3\sqrt{3}} J_0(\sqrt{3}k_0 r) + \left(\frac{4k_0^2}{3} r - \frac{1}{9r} \right) J_1(\sqrt{3}k_0 r) \Bigg] \\ & - k_1 [\sqrt{3} J_0(\sqrt{3}k_0 r) - k_0 r J_1(\sqrt{3}k_0 r)] \Bigg\}\beta_0^{(\pm)} - \mathrm{i}k_0^2 r J_1(\sqrt{3}k_0 r)\beta_0^{(\mp)}. \end{aligned} \tag{5.3}$$

Substitution of (4.4), (5.2) and (5.3), along with the solution (3.4) and (3.5) for the Kelvin waves, into the boundary conditions (4.8) and (4.9) with $\omega_0 = 0$, yields a coupled system of linear algebraic equations for $\alpha_1^{(\pm)}$ and $\beta_1^{(\pm)}$. This is further simplified with the aid of (3.8). Here and hereinafter we use the shorthand notation $K_0 = K_0(k_0)$ and $K_1 = K_1(k_0)$. The resulting equations are collected in matrix form as

$$\begin{bmatrix} -(k_0 K_0 + K_1) & \frac{1}{3}\mathrm{i}[\sqrt{3}k_0 J_0(\sqrt{3}k_0) + J_1(\sqrt{3}k_0)] \\ \mathrm{i}K_1 & J_1(\sqrt{3}k_0) \end{bmatrix} \begin{bmatrix} \alpha_1^{(\pm)} \\ \beta_1^{(\pm)} \end{bmatrix} = \begin{bmatrix} F^{(\pm)} \\ G^{(\pm)} \end{bmatrix}, \tag{5.4}$$

where

$$\begin{aligned} F^{(\pm)} = \mathrm{i}J_1(\sqrt{3}k_0)\Bigg\{ & \left[\pm\frac{\omega_1}{3}\left(4k_0^2 - 5 - \frac{7k_0 K_0}{K_1} \right) - \frac{2k_1}{k_0}\left(1 + \frac{k_0 K_0}{K_1} \right) \right] \beta_0^{(\pm)} \\ & - \left(k_0^2 - \frac{1}{2} - \frac{k_0 K_0}{2K_1} \right)\beta_0^{(\mp)} \Bigg\}, \end{aligned} \tag{5.5}$$

$$\begin{aligned} G^{(\pm)} = J_1(\sqrt{3}k_0)\Bigg\{ & \left[\mp\omega_1\left(\frac{11}{3} + \frac{4k_0 K_0}{K_1} \right) - \frac{2k_1}{k_0}\left(1 + \frac{2k_0 K_0}{K_1} \right) \right] \beta_0^{(\pm)} \\ & + \left(\frac{3}{2} + \frac{2k_0 K_0}{K_1} \right)\beta_0^{(\mp)} \Bigg\}. \end{aligned} \tag{5.6}$$

As is common, the matrix in (5.4) is identical with that to $O(\varepsilon^0)$. In order for (5.4) to make sense, $(F^{(\pm)}, G^{(\pm)})$ must belong to the space of the image of the matrix. This solvability condition demands that

$$\mathrm{i}K_1 F^{(\pm)} + (k_0 K_0 + K_1) G^{(\pm)} = 0. \tag{5.7}$$

Insertion from (5.5) and (5.6) converts (5.7) into homogeneous linear algebraic equations for $\beta_0^{(-)}$ and $\beta_0^{(+)}$:

$$(\omega_1 f \pm k_1 g)\beta_0^{(\pm)} \mp h\beta_0^{(\mp)} = 0, \tag{5.8}$$

k_0	σ_{1max}	Δk_1
0	0.5	∞
2.504982369	0.5707533917	2.145502816
4.349076726	0.5694562098	3.518286549
6.174012330	0.5681222780	4.883945142
7.993536550	0.5671646287	6.247280752
9.810807288	0.5664714116	7.609553122

TABLE 1. The maximum growth rate $\varepsilon\sigma_{1max}$ and the half-width $\varepsilon\Delta k_1$ of the unstable band to $O(\varepsilon)$ for resonance between the helical waves. The case of $\omega_0 = 0$.

where

$$\left.\begin{aligned} f &= 4\left(\frac{k_0K_0}{K_1}\right)^2 + \frac{16k_0K_0}{3K_1} + \frac{4}{3}k_0^2 + 2, \quad g = \frac{4K_0}{K_1}\left(\frac{k_0K_0}{K_1} + 1\right), \\ h &= 2\left(\frac{k_0K_0}{K_1}\right)^2 + \frac{3k_0K_0}{K_1} + k_0^2 + 1. \end{aligned}\right\} \tag{5.9}$$

The flow is unstable when $\mathrm{Im}(\omega_1) > 0$. We reiterate the argument of MS75 and TW76 that non-real ω_1 is permissible only when (5.7) for $m = \pm 1$, being coupled, possesses a non-trivial solution $(\beta_0^{(-)}, \beta_0^{(+)}) \neq \mathbf{0}$, being indicative of parametric resonance. This requirement brings in

$$\omega_1^2 = -(h^2 - k_1^2 g^2)/f^2 = -\sigma_1^2, \tag{5.10}$$

where we have defined $\sigma_1 = |\mathrm{Im}(\omega_1)|$. Because of the reality of f, g and h, moreover $f, g, h > 0$, the instability occurs around every intersection point of the dispersion curves, in a wavenumber range with half width $\varepsilon\Delta k_1$ given by $\Delta k_1 = h/g$. The maximum $\varepsilon\sigma_{1max}$ of the growth rate is attained at $k_1 = 0$ and is $\sigma_{1max} = h/f$. Upon substitution from (5.9), we reach compact formulae:

$$\sigma_{1max} = \frac{3}{2}\left\{2\left(\frac{k_0K_0}{K_1}\right)^2 + \frac{3k_0K_0}{K_1} + k_0^2 + 1\right\} \Big/ \left\{6\left(\frac{k_0K_0}{K_1}\right)^2 + \frac{8k_0K_0}{K_1} + 2k_0^2 + 3\right\}, \tag{5.11}$$

$$\Delta k_1 = \frac{K_1}{4K_0}\left\{2\left(\frac{k_0K_0}{K_1}\right)^2 + \frac{3k_0K_0}{K_1} + k_0^2 + 1\right\} \Big/ \left(\frac{k_0K_0}{K_1} + 1\right). \tag{5.12}$$

It should be borne in mind that the above formulae apply only to the discrete values of k_0 at which the dispersion curves cross the ω_0-axis. We give in table 1 the numerical values of σ_{1max} and Δk_1 for a first few intersection points with $\omega_0 = 0$.

TW76 derived the limiting value $\sigma_{1max} = 1/2$ as $k_0 \to 0$, the instability resulting from the collision of eigenvalues of the isolated branches, and linked this to the two-dimensional result of Moore & Saffman (1971). When the centroid is displaced, the vortex column is swept away as a whole by the shear in the direction parallel to the outward principal axes of strain. The factor $1/2$ originates from the shear strength $\varepsilon/2$ viewed on a large length scale as shown by (2.5). It is worthy of emphasis that the Moore–Saffman–Tsai–Widnall instability encompasses the long-wave instability bearing with Crow's instability (Crow 1970). The infinite bandwidth of the unstable range around $k_0 = 0$ is traced to the fact that $g = 0$ in the limit of $k_0 = 0$. This seemingly singular behaviour is reconciled to the result of Moore & Saffman's analysis that the three-dimensional effect on the growth rate makes its appearance as a correction of

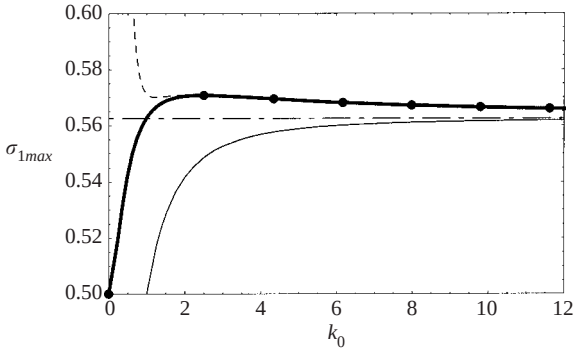

FIGURE 2. The maximum growth rate σ_{1max} as a function of k_0 in the case of $\omega_0 = 0$ as given by (5.11) (a thick solid line) which is valid only at the intersection points, marked with thick dots, of dispersion curves. The short-wave asymptotics (5.13) is included as a dashed line. The horizontal dash-dotted line is the short-wave limit $\sigma_{1max} = 9/16$ obtained by Waleffe (1990). A thin line corresponds to a flow in an elliptic cylinder given by (5.15).

$O(k_1^4)$ (see equation (4.12) of Moore & Saffman 1971). This is beyond the order of the present approximation.

The short-wavelength limit, the other extreme, is handled with no difficulty. As $k_0 \to \infty$, (5.11) and (5.12) become

$$\sigma_{1max} = \frac{9}{16}\left(1 + \frac{1}{12k_0} - \frac{7}{48k_0^2} + \frac{5}{64k_0^3}\right) + O\left(k_0^{-4}\right), \tag{5.13}$$

$$\Delta k_1 = \frac{3k_0}{4}\left(1 + \frac{1}{3k_0} + \frac{5}{24k_0^3}\right) + O\left(k_0^{-3}\right). \tag{5.14}$$

The leading-order term of (5.13) is the well-known value of the growth rate for the elliptical instability elaborated by Waleffe (1990). EL01 obtained this term by an asymptotic expansion of the global analysis of MS75. As (2.5) tells, the strength of shear relevant to the short-wavelength range is ε. The radial wavenumber $\sqrt{3}k_0$ given by (5.1) signifies that the wavenumber vector is inclined at 60° to the z-axis, a salient feature of the elliptical instability (Bayly 1986; Gledzer & Ponomarev 1992; Leweke & Williamson 1998). The second term of (5.13) implies that $O(\varepsilon)$-growth rate overshoots $9/16$ at large values of k_0, in contrast to the case of a bounded geometry for which

$$\sigma_{1max} = \frac{3\left(3k_0^2 + 1\right)}{8\left(2k_0^2 + 1\right)}, \tag{5.15}$$

(Vladimirov *et al.* 1983; Waleffe 1989; Gledzer & Ponomarev 1992; Kerswell 2002). The enhanced growth rate for our unbounded geometry may be attributed to a lift of the constraint of vanishing normal velocity at the edge of the core ($r = R(\theta, \varepsilon)$).

Figures 2 and 3 display, respectively, the growth rate (5.11) and the unstable wavenumber width (5.12) as functions of k_0. The realizable values that occur at the intersection points of dispersion curves are marked with dots. For reference, the short-wave asymptotics (5.13) and (5.14) are included as dashed lines, and the horizontal dash-dotted line in figure 2 is the short-wave limit $\sigma_{1max} = 9/16$. For comparison, figure 2 includes (5.15) as a thin solid line. We observe that the short-wave asymptotics (5.13) and (5.14) can be extrapolated, with an acceptable accuracy, to long wavelengths. Over the entire range of k_0, the most unstable resonance is

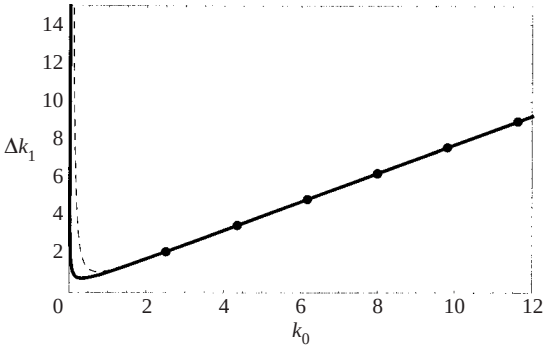

FIGURE 3. The half-width Δk_1 of unstable wavenumber bands as a function of k_0 in the case of $\omega_0 = 0$ as given by (5.12), around the intersection points, marked with thick dots, of dispersion curves. The short-wave asymptotics (5.14) is included as a dashed line.

attained at the intersection point of the first radial modes ($k_0 \approx 2.504982369$) having one radial nodal structure (Tsai & Widnall 1976; Widnall & Tsai 1977; Leweke & Williamson 1998). Except for the long-wave regime, the width Δk_1 of the unstable wavenumber range increases linearly in k_0, being reflective of the broadband nature of the short-wave instability. Neighbouring instability bands overlap with each other in the short-wavelength regime. Roughly speaking, the Moore–Saffman–Tsai–Widnall instability for the stationary waves comprises the long-wave displacement instability and the short-wave instability. The latter is akin to and gives way, in the short-wave limit, to the elliptical instability.

Manipulation of the eigenfunction is straightforward. When restricted to $k_1 = 0$, we see from (5.8) that

$$\beta_0^{(+)}/\beta_0^{(-)} \to -\mathrm{i} \quad \text{as } k_0 \to \infty. \tag{5.16}$$

Taking $\beta_0^{(-)} = \hat{\beta}_0^{(-)} \exp(\mathrm{i}\alpha)$ with α a real constant, curl of (2.7) with $\boldsymbol{v}_0$ substituted from (3.5) yields the vorticity field whose leading-order behaviour is

$$\left.\begin{aligned}
\tilde{\omega}_{0r} &\approx -2\sqrt{3}k_0^2\{J_0(\sqrt{3}k_0 r) + \tfrac{1}{3}J_2(\sqrt{3}k_0 r)\}\cos\hat{z}\cos\left(\theta + \frac{\pi}{4}\right)\hat{\beta}_0^{(-)}, \\
\tilde{\omega}_{0\theta} &\approx 2\sqrt{3}k_0^2\{J_0(\sqrt{3}k_0 r) - \tfrac{1}{3}J_2(\sqrt{3}k_0 r)\}\cos\hat{z}\sin\left(\theta + \frac{\pi}{4}\right)\hat{\beta}_0^{(-)}, \\
\tilde{\omega}_{0z} &\approx -4k_0^2 J_1(\sqrt{3}k_0 r)\sin\hat{z}\cos\left(\theta + \frac{\pi}{4}\right)\hat{\beta}_0^{(-)},
\end{aligned}\right\} \tag{5.17}$$

where

$$\hat{z} = k_0 z + \alpha - \pi/4. \tag{5.18}$$

A choice of $\alpha = \pi/4$ restores Waleffe's construction from local Fourier modes (Waleffe 1990). The shift by $\pi/4$ in θ implies that the vorticity is oriented, on an average, in the direction of maximum strain, and that the rotation centre is displaced in the maximum stretching direction (Leweke & Williamson 1998). This mode has been detected in numerous experiments using a closed container (Gledzer *et al.* 1974, 1975; Chernous'ko 1978; Vladimirov *et al.* 1983; Malkus 1989; Malkus & Waleffe 1991; Eloy *et al.* 2000).

5.2. *The case of* $\omega_0 \neq 0$

If $\omega_0 \neq 0$ for the helical waves and generally if $\omega_0 \neq m+1$ for the $(m, m+2)$ coupling, the disturbance field is free from singularity. In this case also, a general solution of

k_0	ω_0	σ_{1max}	Δk_1
1.263925674	0.4060946928	0.004071827794	0.01193924301
1.750369714	0.5281002276	0.004551168251	0.01962739512
2.113708218	0.5994919938	0.003797861702	0.02140335092
2.410748907	0.6477442773	0.003110938383	0.02154428615
2.665114723	0.6830898257	0.002579186970	0.02112946928
2.889296846	0.7103713246	0.002173139766	0.02051963178
3.300462821	0.1865561255	0.007335004955	0.03664937282
5.173718165	0.1238676584	0.006114894275	0.04520833871
7.016673394	0.0929364737	0.005050467186	0.04952553898
8.847902197	0.0744153565	0.004264381576	0.05212203386

TABLE 2. The maximum growth rate $\varepsilon\sigma_{1max}$ and the half-width $\varepsilon\Delta k_1$ of the unstable band to $O(\varepsilon)$ for resonance between the helical waves. The case of $\omega_0 \neq 0$.

(4.5) and (4.6) finite at $r = 0$ is expressible in a tidy form. A description of the solution and the boundary conditions, along with the solvability conditions, is postponed to Appendix A.

Relevant to the strained helical waves is $m = -1$. On the understanding that the superscript (1) used for the $m = -1$ wave and (2) for the $+1$ wave, $\pi^{(-)}$ and $\pi^{(+)}$ are available by putting $m = -1$ in (A 1) and (A 3), respectively. Alternatively, $\pi^{(+)}$ is built from $\pi^{(-)}$ merely by the replacement

$$\omega_0 \to -\omega_0, \quad \omega_1 \to -\omega_1, \quad \beta_0^{(\pm)} \to -\beta_0^{(\mp)}, \quad \beta_1^{(\pm)} \to -\beta_1^{(\mp)}. \tag{5.19}$$

At the same time, $u_1^{(-)}$ is converted into $-u_1^{(+)}$. As anticipated at the beginning of § 5, (A 1) and (A 3), when restricted to $m = -1$, diverge at $\omega_0 = 0$. In § 5.1, this singularity was cured by virtually making the coefficient $\beta_1^{(\pm)}$ of the homogeneous part in (A 1) and (A 3) infinite so as to compensate for this infinity.

Coexistence of the two types of wave is requisite for parametric resonance. The stipulation that $(\beta_0^{(1)}, \beta_0^{(2)}) \neq \mathbf{0}$ gives rise to $\sigma_1 = |\mathrm{Im}[\omega_1]|$. The maximum growth rate σ_{1max} occurring when $k_1 = 0$ and the half-width Δk_1 of the unstable wavenumber band, if unstable, are found from

$$\sigma_{1max}^2 = -\frac{(\omega_0 - m)^4(\omega_0 - m - 2)^4(\omega_0 - m + 2)(\omega_0 - m - 4)}{64k_0^4(\omega_0 - m - 1)^2}\frac{(h^{(1)})^2}{f^{(1)}f^{(2)}}, \tag{5.20}$$

$$\Delta k_1^2 = -\frac{(\omega_0 - m)^2(\omega_0 - m - 2)^2(\omega_0 - m + 2)(\omega_0 - m - 4)}{64k_0^2(\omega_0 - m - 1)^2} f^{(1)}f^{(2)}(h^{(1)})^2 \Big/ \Big[(\omega_0 - m - 4)f^{(1)}g^{(2)} - (\omega_0 - m + 2)f^{(2)}g^{(1)}\Big]^2, \tag{5.21}$$

where $f^{(1)}$, $f^{(2)}$, $g^{(1)}$, $g^{(2)}$ and $h^{(1)}$ are defined by (A 11)–(A 15).

They are evaluated numerically at many of the intersection points, showing $|\mathrm{Im}\,\omega_1| > 0$ with no exception. Table 2 accommodates the numerical results for a few crossing points, the first six rows along the isolated branch of $m = -1$, and the latter four close to the axis of $\omega_0 = 0$. The evaluated growth rate agrees with that of EL01.

Only the first row ($k_0 \approx 1.263925674$) agrees with the numerics of TW76 up to the first two digits, but for the others, no digit of numerical values coincides with the corresponding one of TW76. This paper takes care to avoid as many cancellations in numerics as possible. It is highly likely that all of the collisions of the eigenvalues

result in instability. In § 7, we put this reasoning on the ground of the Hamiltonian spectral theory.

Comparing with table 1, σ_{1max} at intersection points off the ω_0-axis is drastically smaller, say by two orders of digit, than on the axis. We thus confirm the exclusive prevalence of non-rotating modes. Distinction from the non-rotating resonance is made clear by the short-wave asymptotics. At large values of k_0, (5.20) and (5.21) tend to

$$\sigma_{1max} = \frac{\left(1-\omega_0^2\right)^2\sqrt{9-\omega_0^2}}{64k_0}\left(1+\frac{\omega_0^2-7}{4k_0}-\frac{\omega_0^4-10\omega_0^2-15}{16k_0^2}\right)+O\left(k_0^{-4}\right), \quad (5.22)$$

$$\Delta k_1 = \frac{\left(1-\omega_0^2\right)\sqrt{9-\omega_0^2}}{48}\left(1+\frac{4\omega_0^2-9}{6k_0}+\frac{8\omega_0^4+15\omega_0^2+45}{72k_0^2}\right)+O\left(k_0^{-3}\right). \quad (5.23)$$

In the limit of $k_0 \to \infty$, $\sigma_{1max} = 0$ even if $\omega_0 \to 0$, which is probably the case as evidenced by (B 6) with $m = -1$ (see § 6.2). This exhibits a marked contrast with the behaviour of (5.13) and (5.14). It should be noted that stationarity does not necessarily imply instability.

As the wavelength decreases, rotating instability modes become more and more immaterial, and the elliptical instability alone survives in the limit of $k_0 \to \infty$. The treatment of MS75 and TW76 may, in the short-wavelength regime, give way to the geometric optics approach (Friedlander & Vishik 1991; Lifschitz & Hameiri 1991).

6. Resonance between the $m, m+2$ waves ($m \geqslant 0$)

The helical-wave resonance is not the end of story. Realizability of resonant pairs of higher azimuthal wavenumbers $(m, m+2)$ was speculated by Gledzer & Ponomarev (1992), and (1, 3) resonance was successfully identified by Eloy *et al.* (2000). Among them, (0, 2) mode is considered to be of practical significance. For a bounded flow, the two-dimensional resonance ($k_0 = 0$) is ruled out, and the longest-wave resonance arises for (0, 2). When the Reynolds number is not sufficiently large, the helical-wave resonance, the longest wavelength of which occurs at $k_0 \approx 2.504982369$, is more liable to suffer from viscous dissipation than the (0, 2) resonance, the longest wavelength of which occurs at $k_0 \approx 1.242233570$, as expounded by EL01. Moreover, they revealed that Waleffe's growth rate $9\varepsilon/16$ is approached in the short-wave limit not only of the stationary bending waves but also of specific sequences of $(m, m+2)$ resonance. We are thus requested to pursue all possible pairs of azimuthal wavenumbers $(m, m+2)$.

6.1. *Resonance between the* 0, 2 *waves*

The dispersion relation of the Kelvin waves of $m = 0$ (dashed lines) and $m = 2$ (solid lines) is displayed in figure 4. The isolated branch of $m = 2$, emanating from $\omega_0 = 1$, is drawn with a thick solid line. The frequency range is restricted to $0 \leqslant \omega_0 \leqslant 2$ within which eigenvalue collisions take place.

The growth rate and the unstable band width at an intersection point are found from (5.20) and (5.21) substituted by $m = 0$. Stability is lost at all of the collisions investigated. In table 3, we give the evaluated values for low wavenumbers. The first three rows correspond to the first three intersection points on the isolated mode of $m = 2$. The next three rows are along the first retrograde radial mode of $m = 2$, and the last three along the second.

Following EL01, we count the isolated branch of the $m = 2$ wave as the first, and then the branches of higher radial modes in the order of increasing ω_0 for a given k_0.

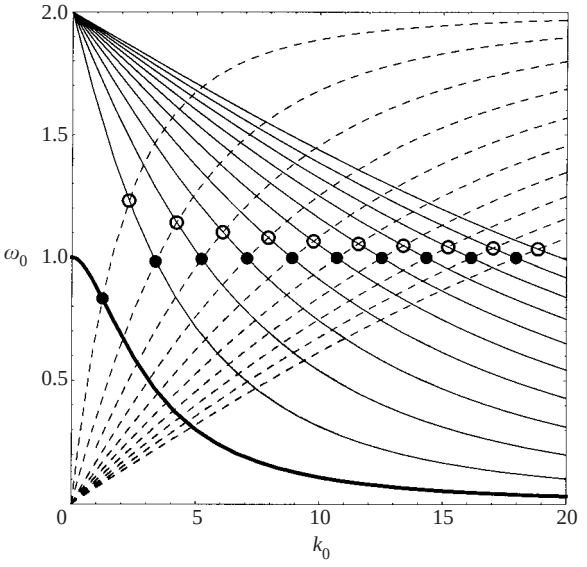

FIGURE 4. Dispersion relation of the axisymmetric wave $m = 0$ (dashed lines) and the elliptic-core wave $m = 2$ (solid lines) on the Rankine vortex. The isolated branch of $m = 2$ is shown by a thick line. ●, principal modes, the intersection points of branches with the same label; ○, intersection points between the ith branch of $m = 0$ and the $(i + 1)$th branch of $m = 2$.

k_0	ω_0	σ_{1max}	Δk_1
•1.242233570	0.8326707799	0.5375272860	1.556281292
2.064157230	0.6708774216	0.07625701507	0.3310664800
2.644269011	0.5697277724	0.02920817805	0.1651547213
◦2.290385144	1.230969403	0.06601417789	0.2406528561
•3.370127336	0.9839106497	0.5652102693	2.781213769
4.173082205	0.8383485487	0.03932264587	0.2434080725
2.863630568	1.374958198	0.01465126151	0.07204545152
◦4.212322721	1.142032400	0.02878428325	0.1761244940
•5.226400945	0.9939985706	0.5668647793	4.167920585

TABLE 3. The maximum growth rate $\varepsilon\sigma_{1max}$ and the half-width $\varepsilon\Delta k_1$ of the unstable band to $O(\varepsilon)$ for (0, 2) resonance.

The axisymmetric wave ($m = 0$) is labelled in the order of decreasing ω_0. The growth rate at an intersection point of the same label, marked with thick dots in figure 4 and table 3, is much larger than that at other intersections. These distinguished pairs are named the *principal modes*. The growth rate of the (0, 2) principal mode is somewhat smaller than, yet comparable to that of the stationary bending waves (−1, 1) given in table 1.

To gain an insight into the instability mechanism, we draw in figure 5 the disturbance vorticity field of $O(\varepsilon^0)$, projected onto the (x, y)-plane, for the first principal mode occurring at $(k_0, \omega_0) \approx (1.242233570, 0.832670779)$. The real parts are extracted from the x and y components of the curl of $\tilde{\mathbf{v}}_0$ given by (2.7). The ratio of the coefficients of the $O(\varepsilon^0)$-disturbance pressure is evaluated from (A 9) and (A 10) to be $\beta_0^{(2)}/\beta_0^{(1)} \approx -1.540522096\,\mathrm{i}$. The chosen values are $\beta_0^{(1)} = 1$, $z = t = 0$. The tendency of alignment

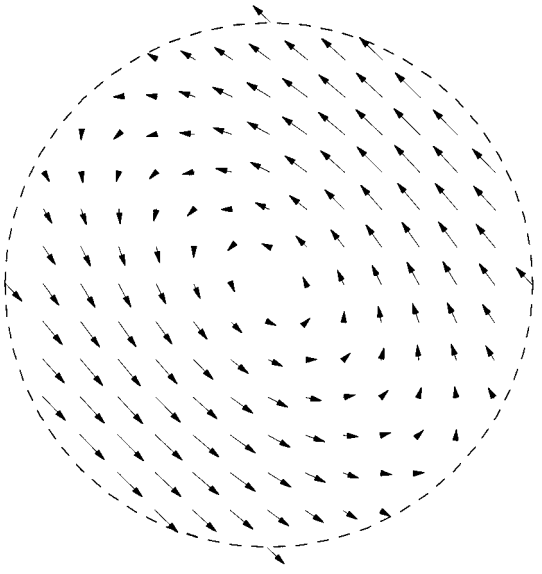

FIGURE 5. Disturbance vorticity field in the (x, y) plane for the first principal mode of the $(0, 2)$ waves excited at $(k_0, \omega_0) \approx (1.242233570, 0.832670779)$. The vortex core cross-section $z = 0$ at $t = 0$ is chosen. The dashed line depicts the core boundary $r = 1$.

of vorticity vector with the direction $\theta = -\pi/4$ and $3\pi/4$ of maximum stretching is clearly recognized.

6.2. *Short-wavelength asymptotics*

The representation (5.20) of growth rate suggests that a resonance pair with ω_0 closest to $m + 1$ is influential. This amounts to the principal modes. As axial wavelength decreases, with m fixed, the growth rate of other modes diminishes and tends to zero in the limit of $k_0 \to \infty$, whereas that of the principal modes asymptotes to $\sigma_{1max} = 9/16$ as verified by EL01. It was also shown that the same limit is taken by the resonance between the ith and the $(i+1)$th branches of the m and the $m+2$ waves, respectively, as m increases. Subsequently, we consolidate this result by extending asymptotic expansions to a higher order in wavelength.

6.2.1. *Large k_0 with m fixed*

Asymptotic expansions of (k_0, ω_0) for intersection points between the $m, m + 2$ waves are made in Appendix B.1. The intersection frequency ω_0 is given by (B 6), and the wavenumber k_0 by a solution of (B 7) for large integers l_1 and l_2 specifying branches of the m and the $m + 2$ waves, respectively.

Among these, the sequence of crossing points between branches of the same label $\Delta l = l_2 - l_1 = 0$ is featured by a fast convergence to $\omega_0 = m + 1$, since the $O(1/k_0)$ term is absent in ω_0. This sequence is exactly the *principal modes*. Substituting from (B 6), (5.20) and (5.21) yield

$$\sigma_{1max} = \frac{9}{16}\left(1 + \frac{1}{12k_0}\right) + O\left(k_0^{-2}\right), \tag{6.1}$$

$$\Delta k_1 = \frac{3k_0}{4}\left(1 + \frac{1}{3k_0}\right) + O\left(k_0^{-1}\right). \tag{6.2}$$

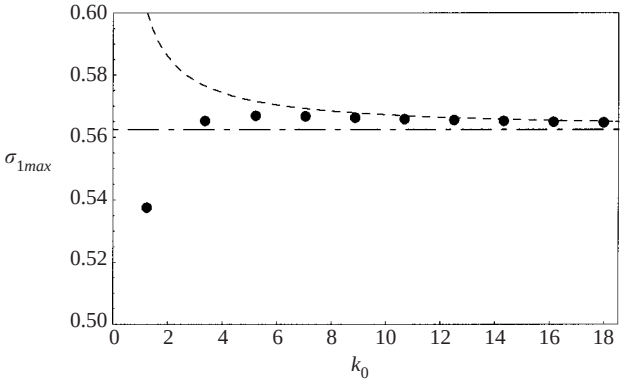

FIGURE 6. The maximum growth rate σ_{1max} as a function of k_0 for the principal modes of (0, 2) resonance (thick dots). The short-wave asymptotics (6.1) is included as a dashed line. The horizontal dash-dotted line is the short-wave limit $\sigma_{1max} = 9/16$.

For a large but finite value of k_0, the growth rate exceeds the limiting value, in accordance with the case of bending waves. Variation of the maximum growth rate σ_{1max} with k_0 is exemplified by (0, 2) resonance in figure 6. The short-wavelength asymptotics (6.1), drawn with a dashed line, fits fairly well for $k_0 > 10$ say. Similarity with figure 2 is recognized, but the maximum growth rate is attained for the third principal mode.

To bring out the point, we derive the asymptotic form of eigenfunction of the principal mode. From (B 1) and its counterpart for the $m+2$ wave, $\eta_1 \sim \eta_2 \to \sqrt{3}k_0$ as $k_0 \to \infty$. From the solvability conditions (A 9) and (A 10), $\beta_0^{(2)}/\beta_0^{(1)} \to -\mathrm{i}$ as $k_0 \to \infty$. Setting $\beta_0^{(1)} = \hat{\beta}_0^{(1)} \exp(\mathrm{i}\alpha)$ with α some real number, the disturbance vorticity of $O(\varepsilon^0)$ is found to be, to the leading order in $1/k_0$,

$$\left.\begin{aligned}
\tilde{\omega}_{0r} &\approx -\frac{k_0^2}{\sqrt{3}}\big\{[6J_{m+1}(\sqrt{3}k_0r) + J_{m-1}(\sqrt{3}k_0r) + J_{m+3}(\sqrt{3}k_0r)]\cos\hat{z}\cos\big(\theta+\tfrac{1}{4}\pi\big)\\
&\quad + [J_{m-1}(\sqrt{3}k_0r) - J_{m+3}(\sqrt{3}k_0r)]\sin\hat{z}\sin\big(\theta+\tfrac{1}{4}\pi\big)\big\}\hat{\beta}_0^{(m)},\\
\tilde{\omega}_{0\theta} &\approx \frac{k_0^2}{\sqrt{3}}\big\{[6J_{m+1}(\sqrt{3}k_0r) - J_{m-1}(\sqrt{3}k_0r) - J_{m+3}(\sqrt{3}k_0r)]\cos\hat{z}\sin\big(\theta+\tfrac{1}{4}\pi\big)\\
&\quad + [J_{m-1}(\sqrt{3}k_0r) - J_{m+3}(\sqrt{3}k_0r)]\sin\hat{z}\cos\big(\theta+\tfrac{1}{4}\pi\big)\big\}\hat{\beta}_0^{(m)},\\
\tilde{\omega}_{0z} &\approx 2k_0^2\big\{[J_m(\sqrt{3}k_0r) - J_{m+2}(\sqrt{3}k_0r)]\sin\hat{z}\cos\big(\theta+\tfrac{1}{4}\pi\big)\\
&\quad - [J_m(\sqrt{3}k_0r) + J_{m+2}(\sqrt{3}k_0r)]\cos\hat{z}\sin\big(\theta+\tfrac{1}{4}\pi\big)\big\}\hat{\beta}_0^{(m)},
\end{aligned}\right\} \tag{6.3}$$

where

$$\hat{z} = k_0 z + (m+1)(\theta - t) + \alpha - \pi/4. \tag{6.4}$$

When specialized to $m = -1$, (6.3) reduces to (5.17). This limiting form is thought of as a superposition of standing waves in θ of the form $\cos(\theta + \pi/4)$ and $\sin(\theta + \pi/4)$, one of which is common with (5.17). The factor $\pi/4$ signifies an overall tendency of the alignment of vorticity vector with stretching directions of the external shear. It is not stationarity but average orientation of disturbance vorticity that is vital to resonance at short wavelengths.

When $\Delta l \neq 0$, $c_1 \neq 0$ and frequency ω_0 approaches $m+1$ less rapidly as k_0 becomes larger. In this case,

$$\sigma_{1max} = \left| \frac{3[4\sqrt{3}(m+1) - \pi\Delta l]}{64\pi\Delta l k_0} + \frac{3}{256\pi^2\Delta l^2 k_0^2}[7\pi^2\Delta l^2 + 32\sqrt{3}(m+1)\pi\Delta l + 16(m+1)^2] \right| + O(k_0^{-3}), \quad (6.5)$$

$$\Delta k_1 = \left| \frac{4\sqrt{3}(m+1) - \pi\Delta l}{16\pi\Delta l} + \frac{1}{32\pi^2\Delta l^2 k_0}[3\pi^2\Delta l^2 + 18\sqrt{3}(m+1)\pi\Delta l + 8(m+1)^2] \right| + O(k_0^{-2}). \quad (6.6)$$

The instability becomes ignorable at very short wavelengths.

6.2.2. *Large k_0 and m with $\eta_1 \sim \eta_2 \sim m$*

The above asymptotic expansions contain m in the coefficients of higher-order terms. They cease to be valid at very large values of m, requiring a separate treatment. As $m \to \infty$, the intersections are arranged so as to satisfy $\eta_1 \sim \eta_2 \sim m$ (EL01).

The asymptotic form of (k_0, ω_0) for the intersection points is found as (B 15) in Appendix B.2. In this, $a_1(<0)$ and $a_2(<0)$ are zeros of the Airy function Ai. The first zero $a_1 \approx -2.338107410$ is tied with the first cograde radial mode of m and $a_2 \approx -2.338107410$ with the first retrograde radial mode of $m+2$.

A rapid approach to $\omega_0 = m+1$ as $m \to \infty$ demands $\Delta a = a_2 - a_1 = 0$. They sit at the crossing points, adjacent to the principal modes, of the ith mode of the m wave and the $(i+1)$th mode of the $m+2$ wave. The latter is equivalent to the ith retrograde radial mode. In figure 4 for (0, 2) resonance, they are marked with circles. The growth rate and the unstable band width for these crossing points are, from (5.20) and (5.21),

$$\sigma_{1max} = \frac{9}{16}\left(1 - \frac{25|a_1|}{12 \times 2^{1/3} m^{2/3}}\right) + O(m^{-1}), \quad (6.7)$$

$$\Delta k_1 = \frac{\sqrt{3}m}{4}\left(1 - \frac{13|a_1|}{12 \times 2^{1/3} m^{2/3}}\right) + O(m^0). \quad (6.8)$$

The limiting value is the same with the principal modes. The eigenfunction has a similar tendency, to leading order, with (6.3), but alignment of the disturbance vorticity vector with the maximum stretching direction is less complete, and there is a difference in the manner of how the limit is approached. In view of $a_1 < 0$, the growth rate is short of 9/16 for a large but finite value of m, as opposed to (6.1).

In case $\Delta a \neq 0$, convergence to $\omega_0 = m+1$ is slower. Consequently, the resonance instability subsides down in the limit of $m \to \infty$ as is seen from

$$\sigma_{1max} = \frac{45}{16 \times 2^{2/3}|\Delta a| m^{1/3}}\left\{1 + \frac{5}{2^{2/3}\Delta a\, m^{1/3}} + \frac{1}{2 \times 2^{1/3} m^{2/3}} \times \left[\frac{25}{\Delta a^2} + \frac{1}{20}\left(49(a_1 + a_2) + \frac{79}{\sqrt{3}}\Delta a\right)\right]\right\} + O(m^{-4/3}), \quad (6.9)$$

$$\Delta k_1 = \frac{5\sqrt{3}m^{2/3}}{4 \times 2^{2/3}|\Delta a|}\left\{1 + \frac{5}{2^{2/3}\Delta a\, m^{1/3}} + \frac{1}{2 \times 2^{1/3} m^{2/3}} \times \left[\frac{25}{\Delta a^2} + \frac{1}{20}\left(29(a_1 + a_2) + \frac{79}{\sqrt{3}}\Delta a\right)\right]\right\} + O(m^{-1/3}). \quad (6.10)$$

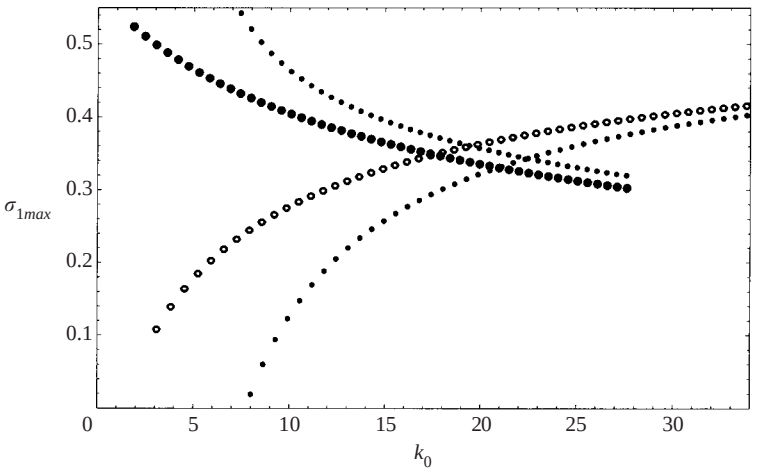

FIGURE 7. The maximum growth rate σ_{1max} as a function of k_0 for the first principal mode (thick dots) and the resonance between the first-first radial modes (circles). The short-wave asymptotics (6.11) and (6.7) for each are included with dotes.

6.2.3. *Large k_0 and m with $\eta_1 \sim m$ but with $\eta_2/(m+2) < 1$*

As long as m is small, the principal modes ($\Delta l = 0$) predominate over the pairs of higher radial modes of the same order ($\Delta a = 0$). As m increases, the principal modes are weakened, while the latter modes are amplified and, at a certain value of m, take the place of the former. The large m behaviour of the crossing points on the isolated branch of $m+2$ takes the form of (B 18). With this, (5.20) and (5.21) yield

$$\sigma_{1max} \approx 3.192216913\, m^{-1/2} + 8.270481688\, a_1 m^{-7/6} + \big(10.64730628 - 0.01203661043\, a_1^3\big) m^{-3/2} + 12.94821843\, a_1^2 m^{-11/6} + O\big(m^{-13/6}\big), \quad (6.11)$$

$$\Delta k_1 \approx 3.612250679\, m^{1/2} + 7.447820120\, a_1 m^{-1/6} + \big(11.20784884 - 0.02749804981\, a_1^3\big) m^{-1/2} + 9.922126238\, a_1^2 m^{-5/6} + O\big(m^{-7/6}\big). \quad (6.12)$$

The first principal mode specified by $a_1 \approx -2.338107410$ is harmless when $m \gg 1$.

To illustrate the alteration of a dominant mode with m, we plot in figure 7 the growth rate σ_{1max} for the first principal mode with thick dots and the resonance mode between the first-first radial branches with circles. The dotted lines are asymptotic expansions (6.11) of the former and (6.7) of the latter, both taking $a_1 \approx -2.338107410$. These points terminate with $(m, m+2) = (50, 52)$. In the passage from $(25, 27)$ to $(26, 28)$, the first principal mode is surpassed by the first-first radial mode.

7. Energetics

Motion of an inviscid fluid is a Hamiltonian dynamical system of infinite degrees of freedom. This section sheds light on the aspect of Hamiltonian spectra, specifically of energetics, relying on Krein's theory of parametric resonance (Krein 1950; MacKay 1986; Dellnitz, Melbourne & Marsden 1992; Marsden 1992).

The circular symmetry of the Rankine vortex prohibits the eigenvalues $-\mathrm{i}\omega_0$ from escaping from the imaginary axis. The symmetry is broken by the pure shear (2.3), a quadrupole field, and two Kelvin waves with azimuthal wavenumber difference 2 can be amplified at a multiple eigenvalue. Here we are reminded of the point that the

spectral stability can be lost only by eigenvalue collisions of positive- and negative-energy waves or by collisions of eigenvalues at 0 (see MacKay 1986 and references therein). Thus, we are tempted to evaluate the energy of the Kelvin waves.

Cairns (1979) invoked an analogy from plasma physics and devised a trick for calculating wave energy that dispenses with a detailed knowledge of the global field (see also Craik 1985). For the moment, we switch off the pure shear. Let the augmented pressure on the vortex, through the interface $r = \eta(\theta, z, t)$ of the form (3.1), acted on by the surrounding fluid be $p_>(z, \theta, t)$, and the pressure on the surrounding fluid acted on by the internal fluid be $p_<(z, \theta, t)$, and pose

$$\{p_>(\theta, z, t),\, p_<(\theta, z, t)\} = \{D_>(k_0, \omega_0),\, D_<(k_0, \omega_0)\}\, A_0^{(m)} \exp(\mathrm{i}(m\theta + k_0 z - \omega_0 t)). \quad (7.1)$$

It is understood that the real part be extracted. Set the difference of the coefficients as

$$D(k_0, \omega_0) = D_>(k_0, \omega_0) - D_<(k_0, \omega_0). \quad (7.2)$$

The requirement of continuity $D = 0$ of pressure across the interface is none other than the dispersion relation. Cairns' formula prescribes the wave energy $E^{(m)}$, per unit length in z, to be

$$E^{(m)} = -\tfrac{1}{2}\pi\omega_0 \frac{\partial D}{\partial \omega_0} \left(A_0^{(m)}\right)^2. \quad (7.3)$$

It seems necessary that the sign be altered from his original formula. Appendix C will exemplify (7.3) with two-dimensional waves on the Rankine vortex.

The pressure P_0 of the Rankine vortex and the disturbance pressure $\pi_0^{(m)}$ inside the core are given, respectively, by (2.2) and (3.5). Putting these together and using (3.9), we can evaluate $P_0 + \pi_0^{(m)} \exp[\mathrm{i}(m\theta + k_0 z - \omega_0 t)]$ at $r = \eta - 0$ to first order in wave amplitude $|A_0^{(m)}|$ complying with the form (7.1), with its coefficient provided by

$$D_< = 1 - \frac{(\omega_0 - m)^2 (\eta_m / k_0)^2 J_{|m|}(\eta_m)}{\eta_m J_{|m|-1}(\eta_m) - [|m| + 2m/(\omega_0 - m)] J_{|m|}(\eta_m)}. \quad (7.4)$$

The disturbance pressure $\pi_0^{(m)}$ in the exterior region is constructed from the disturbance velocity potential $\phi_0^{(m)}$ through $\pi_0^{(m)} = \mathrm{i}\omega_0 \phi_0^{(m)} - \mathrm{i}m\phi_0^{(m)}/r^2$. Evaluation of its boundary value at $r = \eta + 0$ gives

$$D_> = 1 - \frac{(\omega_0 - m)^2 K_{|m|}}{k_0 K_{|m|-1} + |m| K_{|m|}}, \quad (7.5)$$

where $K_{|m|} = K_{|m|}(k_0)$. Substituting (7.5) and (7.4) into (7.2) gives

$$D = (\omega_0 - m)^2 \left\{ \frac{(\eta_m / k_0)^2 J_{|m|}(\eta_m)}{\eta_m J_{|m|-1}(\eta_m) - \left(|m| + \dfrac{2m}{\omega_0 - m}\right) J_{|m|}(\eta_m)} - \frac{K_{|m|}}{k_0 K_{|m|-1} + |m| K_{|m|}} \right\}. \quad (7.6)$$

Provided that $\omega_0 \neq m$ as dictated in (3.6), the condition $D = 0$ indeed regains Kelvin's dispersion relation (3.8). The remaining task is simply to differentiate (7.6) with respect to ω_0 under the constraint of $D = 0$. For this, $\partial \eta_m / \partial \omega_0 = -4k_0^2 / [(\omega_0 - m)^3 \eta_m]$, derivative of (3.3), is used. Further, the Bessel functions are replaced by the modified Bessel functions by repeated use of $D = 0$, and we end up with a representation of

the wave energy in a tidy form:

$$E^{(m)} = \frac{2\pi\omega_0}{\omega_0 - m}\left\{1 + \frac{(k_0/\eta_m)^2 K_{|m|}}{k_0 K_{|m|-1} + |m| K_{|m|}}\left[\frac{2(\omega_0 + m)}{\omega_0 - m} + \left(\frac{m(\omega_0 + m)}{2} + k_0^2\right)\frac{K_{|m|}}{k_0 K_{|m|-1} + |m| K_{|m|}}\right]\right\}\left(A_0^{(m)}\right)^2. \quad (7.7)$$

It is informative to look into the behaviour of (7.7) at long wavelengths. The long-wave behaviour of the dispersion relation (3.8) is due to Kopiev & Chernyshev (1997).

The isolated branch, which is absent for $m = 0$, emerges from a point different from the branches of higher radial modes. Its low-wavenumber behaviour is

$$\omega_0 = \begin{cases} -\frac{1}{2}m\left[\log\left(\frac{2}{k_0}\right) - \gamma + \frac{1}{4}\right]k_0^2 + \cdots & \text{for } |m| = 1, \\ m\left(1 - \frac{1}{|m|}\right) - \frac{m}{2|m|(m^2-1)}k_0^2 + \cdots & \text{for } |m| \geqslant 2, \end{cases} \quad (7.8)$$

where $\gamma \approx 0.5772156649$ is Euler's constant. For higher radial modes,

$$\omega_0 = m \pm \frac{2}{j_n^{(|m|)}}k_0 + \cdots \quad (n = 1, 2, \cdots) \quad \text{for } |m| \geqslant 0, \quad (7.9)$$

where $j_n^{(|m|)}$ is the nth zero of $J_{|m|}(x)$. With these substituted, (7.7) behaves, at small values of k_0, as, for the isolated mode,

$$E^{(m)} = \begin{cases} \left\{\frac{1}{2}\pi\left[\log\left(\frac{2}{k_0}\right) - \gamma + \frac{1}{4}\right]k_0^2 + \cdots\right\}\left(A_0^{(m)}\right)^2 & \text{for } |m| = 1, \\ -\pi\left\{1 - \frac{1}{|m|} + \left[\frac{5}{2|m|} - \frac{1}{m^2} - \frac{1}{2(m^2-1)}\right]k_0^2 + \cdots\right\}\left(A_0^{(m)}\right)^2 & \text{for } |m| \geqslant 2, \end{cases} \quad (7.10)$$

and, for higher radial modes,

$$E^{(m)} = \begin{cases} 2\pi\left\{1 + \cdots\right\}\left(A_0^{(0)}\right)^2 & \text{for } m = 0, \\ \pm\frac{2\pi m j_n^{(|m|)}}{k_0}\left\{1 \pm \frac{2m}{|m| j_n^{(|m|)}}\left(1 + \frac{1}{|m|}\right)k_0 + \cdots\right\}\left(A_0^{(m)}\right)^2 & \text{for } |m| \geqslant 1, \end{cases} \quad (7.11)$$

with the sign being inherited from (7.9).

We point out that the small-wavenumber behaviour (7.10) and (7.11) bears a resemblance to energy of long waves on a vortex ring of uniform-vorticity core obtained by Kop'ev & Chernyshev (2000). The latter took advantage of a different method of employing the Lagrangian variables. Although precise comparison with their result is not straightforward, the sign of energy, a pivotal ingredient, coincides. The limit of a higher radial mode as $k_0 \to 0$ is not looked upon as a planar flow because the axial component w_0 of disturbance velocity is not suppressed in the core. Qualified as the two-dimensional limit is the isolated branch only, and the disturbance energy becomes

$$E^{(m)} = -\pi\left(1 - \frac{1}{|m|}\right)\left(A_0^{(m)}\right)^2 \quad \text{for } |m| \geqslant 1, \quad (7.12)$$

being the limit of (7.10). In Appendix C, we derive (7.12) directly from the total kinetic energy of fluid.

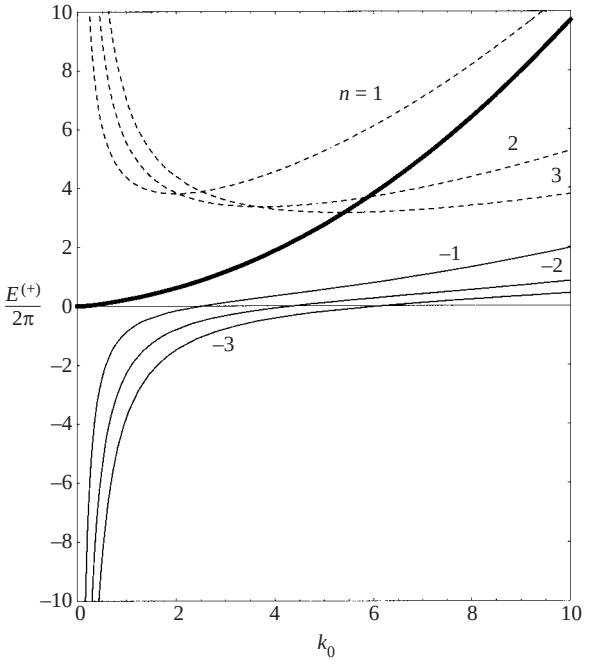

FIGURE 8. The wave energy $E^{(+)}$, normalized by 2π, of the bending wave with $m = 1$ as functions of k_0, as given by (7.7). The solid thick line corresponds to the isolated mode, solid lines to the first three branches of retrograde higher radial modes ($|\omega_0| < 1$), labelled with $n = -1, -2, -3$, and dashed lines to the first three branches of cograde higher radial modes ($|\omega_0| > 1$), labelled with $n = 1, 2, 3$.

With a view to gaining an insight into the result of § 5 and § 6, we sketch in figure 8 the wave energy $E^{(+)}$, divided by 2π, of the left-handed helical wave ($m = 1$) as a function of k_0. The wave energy of $m = -1$ is exactly the same at the same value of k_0 for the same order of branch, as is evident from the invariance property of (7.7) with respect to a replacement $m \to -m$, $\omega_0 \to -\omega_0$. The energy of the isolated mode is drawn with a solid thick line, and that of the first three retrograde radial modes ($|\omega_0| < 1$), counted as $n = -1, -2, -3$, and of the first three cograde radial modes ($|\omega_0| > 1$), counted as $n = 1, 2, 3$, are drawn with solid and dashed lines, respectively. Here, the minus sign is tentatively used in the branch counter for the sake of convenience.

The energy of the isolated mode is positive in the entire wavenumber range. It starts from zero at $k_0 = 0$ and increases monotonically with k_0. The energy of a cograde radial mode is also positive, but it increases without bound as $k_0 \to 0$ and monotonically decreases with k_0 for small values of k_0. The energy of a retrograde radial mode is negative for k_0 smaller than the value at which the dispersion curve transversally crosses the axis of $\omega_0 = 0$. It becomes negative infinity in the limit of $k_0 \to 0$, monotonically increases with k_0, and changes its sign at the intersection point. This singular behaviour in the long-wavelength limit of higher radial modes should not be reckoned as unrealistic. Rather, it is reflective of confinement of wave amplitude in the core. We have postulated a sinusoidal deformation of the core boundary as (3.1). This setting does not agree with the genuinely internal nature, in the long-wave limit, of higher radial modes. Otherwise expressed, given a finite energy, the disturbance of a higher radial mode is confined in the circular core with no influence on its surroundings.

The wave energy of bending waves, calculated from Cairns' formula, exhibits no contradiction with the spectra calculated in § 5. The resonance instability of non-rotating bending waves ($\omega_0 = 0$), the dominant ones, manifests itself at a degenerate eigenvalue with multiplicity two whose eigenfunction has zero energy. The resonance instability of rotating bending waves ($\omega_0 \neq 0$) stems from an eigenvalue collision either between the isolated mode of positive energy and a retrograde higher mode of negative energy or between a positive-energy and a negative-energy retrograde higher modes.

The energy of the axisymmetric wave ($m = 0$) is positive for all branches. As a rule, for $m \geqslant 2$, the isolated mode and a retrograde radial mode, for which ω_0 is a decreasing function of k_0, have negative energy, while the energy of a cograde radial mode, for which ω_0 is an increasing function, is positive. It follows that, for a pair $(m, m+2)$ $(m \geqslant 0)$, multiple eigenvalues necessarily occur between waves of opposite signed energies. This lends some support to the fact that every eigenvalue collision leads to instability.

8. Conclusion

We have re-examined the three-dimensional linear stability problem of a straight vortex tube exposed to a pure shear flow, originally solved by Moore & Saffman (1975), Tsai & Widnall (1976) and Eloy & Le Dizès (2001). We have found that the model of TW76 and EL01 is solvable; when the vorticity of the basic flow is uniform, an expression in terms only of the Bessel and modified Bessel functions is afforded for the disturbance flow field. The explicit solution has been exploited to develop a thorough analysis of parametric resonance instability between the Kelvin waves with azimuthal wavenumber m and $m+2$, mediated by the pure shear. The advantage of an explicit solution is twofold.

The obvious advantage is to make feasible an efficient computation with a high accuracy. Cancellations of large numbers have been effected to a great extent by hand. Thereby we could amend numerical inadequacy in TW76 that occurred for multiple eigenvalues of the rotating bending waves ($\omega_0 \neq 0$). Our numerical results rule out the possibility for persistence of stability when a multiple eigenvalue occurs. The wavenumber range of instability has attracted less attention. The broadening of the unstable band with k_0 is demonstrated both numerically and asymptotically for the first time.

Secondly, the closed form of solution manifests the mathematical structure lying behind the distinguished status shared by non-rotating bending waves. The singularity at $\omega_0 = 0$ of the general solution (A 1)–(A 4) unveils the overwhelmingly large growth rate of non-rotating resonance. Moreover, the crossover to its extremes is clearly seen. The analytical formulae, specifically (5.11), clarify the behaviour over a wide wavenumber range. Strictly speaking, the intuitive argument provided by Widnall *et al.* (1974) and MS75 is of limited use to the instability with respect to displacement of the vorticity centroid in the long-wave limit, for which $\varepsilon\sigma_{1max} = \varepsilon/2$ (table 1). The transition to the other extreme is comprehensible as (5.13). The short-wave limit is $\varepsilon\sigma_{1max} = 9\varepsilon/16$ for the elliptical instability subject to local shear of strength ε. Moreover, it is found that the growth rate is larger than the limit for a large but finite value of k_0. The augmented growth rate is peculiar to an open geometry. This trend carries over to the principal modes of $(m, m+2)$ resonance as is read off from (6.1). In a different short-wave limit of $m \sim \eta_1 \sim \eta_2 \to \infty$, the growth rate is the same in the limit but is smaller at a finite value of m as shown by (6.7). The θ-dependence of vorticity field (6.3) accounts for the dominance of these modes. In a practical flow,

viscosity acts in favour of small axial and azimuthal wavenumbers. The other modes, the rotating modes ($\omega_0 \neq 0$) for $(-1, 1)$ resonance and the ones with frequency less close to $\omega_0 = m+1$ for $(m, m+2)$ resonance, have very small growth rates and subside down in the short-wave limit.

In order to reinforce our numerical results, we have evaluated in § 7 the excess energy of the Kelvin waves for general azimuthal and axial wavenumbers by resorting to Cairns' formula. It has been confirmed that the non-rotating resonance instability of $m = \pm 1$ is tied to a multiple eigenvalue of zero-energy modes, while the rotating resonance instability of $(m, m+2)$ is tied to an eigenvalue collision of positive and negative-energy modes. In a rigorous sense, the energy criterion is a necessary condition for instability, but in effect serves as a sufficient condition as well. The aspect of symmetry may bring us a precise understanding of this accidental coincidence (Dellnitz *et al.* 1992; Guckenheimer & Mahalov 1992).

Finally, some comments upon related topics are in order. Along the same line of analysis, we can address the linear stability of Kelvin's vortex ring, an axisymmetric vortex ring with uniform vortical core (Fukumoto & Hattori 2003*a*, *b*). It has been shown that curvature effect triggers a novel parametric resonance between the $m, m+1$ waves. Although the formulation was presented by Widnall & Tsai (1977), this possibility has gone untouched. Contrary to the present case, multiple eigenvalues do not necessarily result in instability. Knowledge of mode energy holds the key to making a distinction between resonant and non-resonant collisions of eigenvalues. In the short-wave limit, the geometric optics approach captures the local resonance structure (Hattori & Fukumoto 2003).

The compact solution of the linearized Euler equations has much in its favour in making headway to a weakly nonlinear stability analysis (cf. Malkus & Waleffe 1991; Gledzer & Ponomarev 1992; Kerswell 2002). A possible Hamiltonian normal form for the weakly nonlinear development of wave amplitude was derived by Guckenheimer & Mahalov (1992). The present solution will facilitate the reliable calculation of its coefficients.

The rigid-body rotating core is a rare model which admits an analytical handling. An extension to a Gaussian distribution of vorticity was accomplished by Eloy & Le Dizès (1999). However, they paid attention only to the non-rotating resonance. For rotating waves, even the spectra on an unstrained core with distributed vorticity are little understood. Continuous as well as discrete spectra will take part in the wave dynamics. Possible parametric resonance between discrete and continuous eigenmodes may lead to understanding of the stability characteristics which is left for a further investigation (cf. Iga 1999; Yoshida & Tatsuno 2003).

I am grateful to Y. Hattori for helpful discussions. This work was supported in part by a Grant-in-Aid for Scientific Research from the Japan Society for the Promotion of Science.

Appendix A. Disturbance field and the solvability conditions for the m, $m+2$ waves

This Appendix collects the solution for the disturbance field $\pi_1^{(m)}$, $\pi_1^{(m+2)}$ and $u_1^{(m)}$, $u_1^{(m+2)}$ in the core, the boundary conditions and the solvability conditions for general azimuthal wavenumbers m and $m+2$. For brevity, we use super- and subscripts 1 and 2 in place of m and $m+2$, respectively. To derive the expressions that follow, some symbolic manipulation by computer would be indispensable.

Provided that $\omega_0 \neq m+1$, a general solution of (4.5) for m, finite at $r=0$, is found to be

$$\pi_1^{(1)} = J_m(\eta_1 r)\beta_1^{(1)} + \left\{ \frac{4k_0^2\omega_1}{(\omega_0-m)^3\eta_1} - \frac{\eta_1}{k_0}k_1 \right\} r J_{m+1}(\eta_1 r)\beta_0^{(1)} + \frac{1}{4}\left\{ \frac{(\omega_0-m)^2(\omega_0-m+2)(\omega_0-m-4)}{8(\omega_0-m-1)} J_m(\eta_2 r) - \eta_2 r J_{m+1}(\eta_2 r) \right\}\beta_0^{(2)}, \quad \text{(A 1)}$$

where $\beta_1^{(1)}$ is a constant, and it is kept in view that $\eta_1 = \eta_m$ and $\eta_2 = \eta_{m+2}$. Returning to the Euler equations, (4.3), we obtain

$$\begin{aligned} u_1^{(1)} = {} & \frac{\mathrm{i}}{\omega_0-m+2}\left\{ -\frac{m}{r}J_m(\eta_1 r) + \frac{\omega_0-m}{\omega_0-m-2}\eta_1 J_{m+1}(\eta_1 r) \right\}\beta_1^{(1)} \\ & + \frac{\mathrm{i}\omega_1}{\omega_0-m+2}\left\{ \left[\frac{m}{(\omega_0-m+2)r} - \frac{4k_0^2 r}{(\omega_0-m)^2(\omega_0-m-2)} \right] J_m(\eta_1 r) \right. \\ & \left. - \frac{\omega_0^3 - 3m\omega_0^2 + (3m^2+4m+4)\omega_0 - m^3 - 4m^2 + 4m}{(\omega_0-m)(\omega_0-m+2)(\omega_0-m-2)^2}\eta_1 J_{m+1}(\eta_1 r) \right\}\beta_0^{(1)} \\ & - \mathrm{i}k_1\left\{ \frac{k_0 r}{\omega_0-m}J_m(\eta_1 r) + \frac{m}{k_0(\omega_0-m-2)}\eta_1 J_{m+1}(\eta_1 r) \right\}\beta_0^{(1)} \\ & + \frac{\mathrm{i}}{4}\left\{ -\left[\frac{m(\omega_0-m)^2(\omega_0-m-4)}{8(\omega_0-m-1)r} + \frac{k_0^2 r}{\omega_0-m-2} \right] J_m(\eta_2 r) + \frac{1}{8}\left[\omega_0^2 - (2m+1)\omega_0 \right. \right. \\ & \left. \left. + m^2 + m - 5 - \frac{8}{\omega_0-m} + \frac{3}{\omega_0-m-1} - \frac{8(m+1)}{\omega_0-m-4} \right] \eta_2 J_{m+1}(\eta_2 r) \right\}\beta_0^{(2)}. \quad \text{(A 2)} \end{aligned}$$

Likewise, for $m+2$, we have

$$\pi_1^{(2)} = J_{m+2}(\eta_2 r)\beta_1^{(2)} - \left\{ \frac{4k_0^2\omega_1}{(\omega_0-m-2)^3\eta_2} - \frac{\eta_2}{k_0}k_1 \right\} r J_{m+1}(\eta_2 r)\beta_0^{(2)} + \frac{1}{4}\left\{ \eta_1 r J_{m+1}(\eta_1 r) - \frac{(\omega_0-m-2)^2(\omega_0-m+2)(\omega_0-m-4)}{8(\omega_0-m-1)} J_{m+2}(\eta_1 r) \right\}\beta_0^{(1)}, \quad \text{(A 3)}$$

$$\begin{aligned} u_1^{(2)} = {} & \frac{\mathrm{i}}{\omega_0-m-4}\left\{ -\frac{\omega_0-m-2}{\omega_0-m}\eta_2 J_{m+1}(\eta_2 r) + \frac{m+2}{r}J_{m+2}(\eta_2 r) \right\}\beta_1^{(2)} + \frac{\mathrm{i}\omega_1}{\omega_0-m-4} \\ & \times \left\{ \frac{\omega_0^3 - 3(m+2)\omega_0^2 + (3m^2+8m+8)\omega_0 - m^3 - 2m^2 + 8m + 16}{(\omega_0-m)^2(\omega_0-m-2)(\omega_0-m-4)}\eta_2 J_{m+1}(\eta_2 r) \right. \\ & \left. - \left[\frac{m+2}{(\omega_0-m-4)r} + \frac{4k_0^2 r}{(\omega_0-m)(\omega_0-m-2)^2} \right] J_{m+2}(\eta_2 r) \right\}\beta_0^{(2)} \\ & - \mathrm{i}k_1\left\{ \frac{m+2}{k_0(\omega_0-m)}\eta_2 J_{m+1}(\eta_2 r) + \frac{k_0 r}{\omega_0-m-2}J_{m+2}(\eta_2 r) \right\}\beta_0^{(2)} \\ & + \frac{\mathrm{i}}{4}\left\{ \frac{1}{8}\left[\omega_0^2 - (2m+3)\omega_0 + m^2 + 3m - 3 - \frac{3}{\omega_0-m-1} \right. \right. \end{aligned}$$

$$+\frac{8}{\omega_0-m-2}-\frac{8(m+1)}{\omega_0-m+2}\Bigg]\eta_1 J_{m+1}(\eta_1 r)$$
$$-\left[\frac{(m+2)(\omega_0-m-2)^2(\omega_0-m+2)}{8(\omega_0-m-1)r}+\frac{k_0^2 r}{\omega_0-m}\right]J_{m+2}(\eta_1 r)\Bigg\}\beta_0^{(1)}, \tag{A 4}$$

where $\beta_1^{(2)}$ is a constant.

For the m wave, the boundary conditions (4.8) are converted into linear algebraic equations for $\alpha_1^{(1)}$ and $\beta_1^{(1)}$:

$$\begin{bmatrix} mK_m - k_0 K_{m+1} & \dfrac{\mathrm{i}}{\omega_0-m+2}\left[mJ_m(\eta_1)-\dfrac{\omega_0-m}{\omega_0-m-2}\eta_1 J_{m+1}(\eta_1)\right] \\ -\mathrm{i}(\omega_0-m)K_m & J_m(\eta_1) \end{bmatrix}\begin{bmatrix}\alpha_1^{(1)}\\ \beta_1^{(1)}\end{bmatrix}=\begin{bmatrix}F^{(1)}\\ G^{(1)}\end{bmatrix}, \tag{A 5}$$

where $K_m = K_m(k_0)$ and $K_{m+1} = K_{m+1}(k_0)$. Elimination of $J_{m+1}(\eta_1)$, by use of the dispersion relation (3.8), simplifies $F^{(1)}$ and $G^{(1)}$. The matrix in (A 5) is singular. Hence $F^{(1)}$ and $G^{(1)}$ must satisfy the solvability condition, in order for (A 5) to have a solution for $(\alpha_1^{(1)}, \beta_1^{(1)})$,

$$\mathrm{i}(\omega_0-m)F^{(1)}+\left(m-\frac{k_0K_{m+1}}{K_m}\right)G^{(1)}=0. \tag{A 6}$$

Repeating the same procedure, the solvability condition for the $m+2$ wave is obtained as

$$\mathrm{i}(\omega_0-m-2)F^{(2)}-\left(m+2+\frac{k_0K_{m+1}}{K_{m+2}}\right)G^{(2)}=0. \tag{A 7}$$

Again, $F^{(2)}$ and $G^{(2)}$ are simplified by eliminating $J_{m+1}(\eta_2)$, using the following form of the dispersion relation:

$$J_{m+1}(\eta_2)=\left\{\frac{k_0K_{m+1}}{K_{m+2}}-\frac{2(m+2)}{\omega_0-m-4}\right\}\frac{\eta_2}{k_0^2}J_{m+2}(\eta_2). \tag{A 8}$$

These conditions furnish homogeneous linear algebraic equations for $\beta_0^{(1)}$ and $\beta_0^{(2)}$:

$$\left\{\frac{\omega_1 f^{(1)}}{(\omega_0-m)(\omega_0-m+2)}+\frac{2k_1}{k_0}(\omega_0-m-2)g^{(1)}\right\}\beta_0^{(1)}$$
$$+\frac{(\omega_0-m)^3J_{m+2}(\eta_2)}{8k_0^2(\omega_0-m-1)J_m(\eta_1)}h^{(1)}\beta_0^{(2)}=0, \tag{A 9}$$

$$\frac{(\omega_0-m-2)^3J_m(\eta_1)}{8k_0^2(\omega_0-m-1)J_{m+2}(\eta_2)}h^{(1)}\beta_0^{(1)}$$
$$+\left\{\frac{\omega_1 f^{(2)}}{(\omega_0-m-2)(\omega_0-m-4)}+\frac{2k_1}{k_0}(\omega_0-m)g^{(2)}\right\}\beta_0^{(2)}=0, \tag{A 10}$$

where

$$f^{(1)}=m\{(\omega_0-m-2)[\omega_0^2-2(m+1)\omega_0+m^2-6m-4]-8(m+1)\}+2k_0^2(\omega_0-m)^2$$
$$+4\{(\omega_0-m-2)[(m+1)\omega_0-m^2+3m+2]+4(m+1)\}\frac{k_0K_{m+1}}{K_m}$$
$$-2(\omega_0-m+2)(\omega_0-m-2)\left(\frac{k_0K_{m+1}}{K_m}\right)^2, \tag{A 11}$$

$$f^{(2)} = (m+2)\{(\omega_0 - m)[\omega_0^2 - 2(m+1)\omega_0 + m^2 + 10m + 12] - 8(m+1)\}$$
$$+ 2k_0^2(\omega_0 - m - 2)^2 - 4\{(\omega_0 - m)[(m+1)\omega_0 - m^2 - 7m - 8] + 4(m+1)\}\frac{k_0 K_{m+1}}{K_{m+2}}$$
$$- 2(\omega_0 - m)(\omega_0 - m - 4)\left(\frac{k_0 K_{m+1}}{K_{m+2}}\right)^2, \tag{A 12}$$

$$g^{(1)} = -\left(m - \frac{k_0 K_{m+1}}{K_m}\right)\left[m(\omega_0 - m - 1) + \frac{k_0 K_{m+1}}{K_m}\right], \tag{A 13}$$

$$g^{(2)} = \left(m + 2 + \frac{k_0 K_{m+1}}{K_{m+2}}\right)\left[(m+2)(\omega_0 - m - 1) + \frac{k_0 K_{m+1}}{K_{m+2}}\right], \tag{A 14}$$

$$h^{(1)} = (\omega_0 - m)(\omega_0 - m - 2)\left[m(m+1)(m+2) - \frac{k_0^2(\omega_0 + 2m + 2)}{2}\right] - k_0^4(\omega_0 - m - 1)$$
$$- (m+1)(\omega_0 - m)(\omega_0 - m - 2)[(m+1)\omega_0 - (m^2 + 2m - 2)]\frac{k_0 K_{m+1}}{K_{m+2}}$$
$$- [(m+1)^2(m+2)(\omega_0 - m)(\omega_0 - m + 2)(\omega_0 - m - 2) - k_0^4(\omega_0 - m - 1)]\frac{K_{m+1}^2}{K_m K_{m+2}}. \tag{A 15}$$

Appendix B. Short-wavelength asymptotics of the dispersion relation

We shall carry through asymptotic expansions of (k_0, ω_0) for intersection points between dispersion curves of the m and the $m+2$ waves, valid at large k_0 in Appendix B.1, and valid at large m with $\eta_1 \sim \eta_2 \sim m$ in Appendix B.2. This Appendix is an extension of EL01 to a higher order.

B.1. *Large k_0 with m fixed*

Anticipating that $\omega_0 \to m + 1$ as $k_0 \to \infty$ (EL01), we pose $\omega_0 = m + 1 + \sum_{i=1} c_i k_0^{-i}$, an expansion in powers of $1/k_0$, and determine the constants c_1, c_2 and c_3.

For the m wave, (3.3) is expanded as

$$\eta_1 = \sqrt{3}k_0 - \frac{4c_1}{\sqrt{3}} - \frac{2(6c_2 - 5c_1^2)}{3\sqrt{3}k_0} - \frac{4(9c_3 - 15c_1c_2 + 8c_1^3)}{9\sqrt{3}k_0^2} + O(k_0^{-3}). \tag{B 1}$$

Using the large-wavenumber asymptotic expansions

$$\frac{K_{m+1}(k_0)}{K_m(k_0)} = 1 + \left(m + \frac{1}{2}\right)\frac{1}{k_0} + \left(\frac{m^2}{2} - \frac{1}{8}\right)\frac{1}{k_0^2} + O(k_0^{-3}),$$
$$J_m(\eta_1) = \left\{1 - \frac{16m^4 - 40m^2 + 9}{128\eta_1^2}\right\}\cos\left(\eta_1 - \frac{2m+1}{4}\pi\right)$$
$$- \left(\frac{m^2}{2} - \frac{1}{8}\right)\frac{1}{\eta_1}\sin\left(\eta_1 - \frac{2m+1}{4}\pi\right) + O(\eta_1^{-3}), \tag{B 2}$$

and a similar one for $J_{m+1}(\eta_1)$ (Abramowitz & Stegun 1965), (3.8) is expanded, for $\omega_0 > m$, as

$$k_0 - \frac{4c_1}{3} - \frac{4}{3k_0}\left(c_2 - \frac{5c_1^2}{6}\right) - \frac{4}{3k_0^2}\left(c_3 - \frac{5c_1c_2}{3} + \frac{8c_1^3}{9}\right)$$
$$= \frac{\pi}{\sqrt{3}}\left\{l_1 + \frac{1}{2}\left(m - \frac{1}{6}\right)\right\} + \frac{1}{3k_0}\left(c_1 - \frac{4m^2+4m+3}{8}\right)$$
$$+\frac{1}{3k_0^2}\left\{c_2 + \frac{c_1^2}{6} - \frac{(m+1)(4m+3)c_1}{6} - \frac{2m^2-4m-3}{8}\right\} + O(k_0^{-3}), \quad \text{(B 3)}$$

where l_1 is a large integer that labels branches of the m wave, with $l_1 = 1$ corresponding to the first cograde radial mode ($\omega_0 > m$). Proceeding similarly to the $m+2$ wave, the asymptotic expansion of (A 8) is deduced, for $\omega_0 < m+2$, as

$$k_0 + \frac{4c_1}{3} + \frac{4}{3k_0}\left(c_2 + \frac{5c_1^2}{6}\right) + \frac{4}{3k_0^2}\left(c_3 + \frac{5c_1c_2}{3} + \frac{8c_1^3}{9}\right)$$
$$= \frac{\pi}{\sqrt{3}}\left\{l_2 + \frac{1}{2}\left(m - \frac{1}{6}\right)\right\} - \frac{1}{3k_0}\left(c_1 + \frac{4m^2+12m+11}{8}\right)$$
$$-\frac{1}{3k_0^2}\left\{c_2 - \frac{c_1^2}{6} - \frac{(m+1)(4m+5)c_1}{6} + \frac{2m^2+12m+13}{8}\right\} + O(k_0^{-3}), \quad \text{(B 4)}$$

where l_2 is a large labelling integer with $l_2 = 1$ corresponding to the isolated mode.

By finding the constants c_1, c_2 and c_3 that fulfil (B 3) and (B 4) at the same time, we obtain an asymptotic expression of ω_0 for an intersection point. Introducing the notation

$$\Delta l = l_2 - l_1, \quad \text{(B 5)}$$

the intersection frequency is expressed as

$$\omega_0 = m + 1 + \frac{\sqrt{3}\pi\Delta l}{8k_0} - \frac{1}{32k_0^2}[\sqrt{3}\pi\Delta l + 4(m+1)]$$
$$-\frac{1}{16k_0^3}\left\{\frac{\pi^3\Delta l^3}{4\sqrt{3}} - \frac{\pi\Delta l}{\sqrt{3}}\left[(m+1)^2 + \tfrac{3}{8}\right] + \tfrac{7}{2}(m+1)\right\} + O(k_0^{-4}). \quad \text{(B 6)}$$

According to (B 3) and (B 4), the corresponding wavenumber k_0 is found by solving iteratively

$$k_0 = \frac{\pi}{2\sqrt{3}}(l_1 + l_2 + m - \tfrac{1}{6}) - \frac{1}{24k_0}\left\{\frac{5\pi^2\Delta l^2}{4} + 4(m+1)^2 + 3\right\}$$
$$+\frac{1}{24k_0^2}\left\{\frac{11\pi^2\Delta l^2}{16} + \sqrt{3}(m+1)\pi\Delta l - 2(m+1)^2 - 3\right\} + O(k_0^{-3}). \quad \text{(B 7)}$$

B.2. *Large k_0 and m with $\eta_1 \sim \eta_2 \sim m$*

The increasing power of m with order of expansion in the coefficients of (B 6) suggests that a separate treatment is necessary for large values of m. It is expedient for our purpose to eliminate ω_0, in terms of the radial wavenumber η_1, from the dispersion

relation (3.8) for the m wave, leaving

$$\left\{\frac{\eta_1}{k_0}\frac{K'_m(k_0)}{K_m(k_0)} - \frac{m}{\eta_1}\sqrt{1+\left(\frac{\eta_1}{k_0}\right)^2}\right\}J_m(\eta_1) + J'_m(\eta_1) = 0, \tag{B 8}$$

where a prime stands for differentiation with respect to the argument. The dominant mode, $\omega_0 \sim m+1$, occurs for $\eta_1 \sim m$. The asymptotics of the Bessel functions, valid for this regime, are

$$J_m\big(m+\xi m^{1/3}\big) = 2^{1/3}\left(\frac{1}{m^{1/3}} - \frac{\xi}{5m}\right)\mathrm{Ai}\big(-2^{1/3}\xi\big) + \frac{3\times 2^{2/3}\xi^2}{10m}\mathrm{Ai}'\big(-2^{1/3}\xi\big) + O\big(m^{-5/3}\big), \tag{B 9}$$

$$\frac{K'_m(k_0)}{K_m(k_0)} = -\frac{(1+\kappa^2)^{1/2}}{\kappa}\left\{1 + \frac{\kappa^2}{2m(1+\kappa^2)^{3/2}}\right\} + O(m^{-2}), \tag{B 10}$$

where Ai is the Airy function, ξ is some constant of order unity and

$$\kappa = k_0/m. \tag{B 11}$$

Then η_1 is gained from (B 8) in the form of a power series in $m^{-1/3}$ as

$$\eta_1 = m - \frac{a_1}{2^{1/3}}m^{1/3} + \frac{\kappa^2}{(\kappa+1)(\kappa^2+1)^{1/2}} + \frac{3a_1^2}{10\times 2^{2/3}m^{1/3}} - \frac{a_1\kappa^2(\kappa^4-3\kappa^2-3\kappa-3)}{3\times 2^{1/3}m^{2/3}(\kappa+1)^3(\kappa^2+1)^{3/2}} + O(m^{-1}), \tag{B 12}$$

where a_1 is a zero of the Airy function Ai.

Repetition of the same procedure for the dispersion relation of the $m+2$ wave

$$\left\{\frac{\eta_2}{k_0}\frac{K'_{m+2}(k_0)}{K_{m+2}(k_0)} + \frac{m+2}{\eta_2}\sqrt{1+\left(\frac{\eta_2}{k_0}\right)^2}\right\}J_{m+2}(\eta_2) + J'_{m+2}(\eta_2) = 0, \tag{B 13}$$

yields

$$\eta_2 = m - \frac{a_2}{2^{1/3}}m^{1/3} + 2 - \frac{\kappa^2}{(\kappa-1)(\kappa^2+1)^{1/2}} + \frac{3a_2^2}{10\times 2^{2/3}m^{1/3}} + \frac{a_2}{3\times 2^{1/3}m^{2/3}}\left\{\frac{\kappa^2(\kappa^4-3\kappa^2+3\kappa-3)}{(\kappa-1)^3(\kappa^2+1)^{3/2}} - 2\right\} + O(m^{-1}), \tag{B 14}$$

where a_2 is a zero of Ai.

Remembering the notation $\eta_1 = \eta_m$ and $\eta_2 = \eta_{m+2}$ with η_m defined by (3.3), the crossing point (ω_0, k_0) of dispersion curves of the m, $m+2$ waves is obtained as the simultaneous solution of (B 12) and (B 14) as

$$k_0 = \frac{m}{\sqrt{3}} - \frac{a_1+a_2}{2\times 2^{1/3}\sqrt{3}}m^{1/3} + \frac{1}{4} + \frac{1}{\sqrt{3}} - \frac{a_1^2-50a_1a_2+a_2^2}{160\times 2^{2/3}\sqrt{3}m^{1/3}} - \frac{1}{16\times 2^{1/3}m^{2/3}}\left(\frac{a_1+a_2}{2} + \frac{61a_1-45a_2}{3\sqrt{3}}\right) + O(m^{-1}),$$

$$\omega_0 = m + 1 - \frac{3(a_2-a_1)}{8\times 2^{1/3}m^{2/3}} + \frac{15}{16m} - \frac{3\big(a_2^2-a_1^2\big)}{40\times 2^{2/3}m^{4/3}} + \frac{7a_1+39a_2+21\sqrt{3}(a_2-a_1)}{64\times 2^{1/3}m^{5/3}} + O(m^{-2}). \tag{B 15}$$

B.3. *Large k_0 and m with $\eta_1 \sim m$ but with $\eta_2/(m+2) < 1$*

The isolated mode of the $m+2$ wave drops out from the preceding large m analysis. For this mode, $Z = \eta_2/(m+2)$ asymptotes to a constant smaller than unity as m is increased. Validated for $Z < 1$ is Debye's asymptotic expansions given by

$$\frac{J'_{m+2}(\eta_2)}{J_{m+2}(\eta_2)} = \frac{(1-Z^2)^{1/2}}{Z}\left\{1 + \frac{Z^2}{2(m+2)(1-Z^2)^{1/2}}\right\} + O(m^{-2}). \tag{B 16}$$

For K'_{m+2}/K_{m+2}, (B 10), with m replaced by $m+2$, holds true. With this form, (B 13) is solved for Z and then for η_2, resulting in

$$\eta_2 = \frac{\kappa(3-\kappa^2)^{1/2}}{(\kappa^2-1)^{1/2}}m - \frac{\kappa^3[\kappa^2(\kappa^2-1) - 8(\kappa^2+1)^{1/2}]}{(3-\kappa^2)^{1/2}(\kappa^2+1)^2} + O(m^{-1}). \tag{B 17}$$

Combination of (B 17) with (B 12) gives rise to

$$\begin{aligned} k_0 &\approx 0.4933773767\, m - 0.2996728474\, a_1 m^{1/3} + 0.2915996919 \\ &\quad + 0.002190766286\, a_1^2 m^{-1/3} - 0.3559416194\, a_1 m^{-2/3} + O(m^{-1}), \\ \omega_0 &\approx m + 0.8849120053 + 0.1325920502\, a_1 m^{-2/3} + 0.3165890161 m^{-1} \\ &\quad - 0.03335383087\, a_1^2 m^{-4/3} - 0.2741735953\, a_1 m^{-5/3} + O(m^{-2}). \end{aligned} \tag{B 18}$$

For consistency, we confirm that

$$Z \sim 0.7346073926 \quad \text{as } m \to \infty. \tag{B 19}$$

Appendix C. Energy of planar Kelvin waves

We illustrate the applicability of Cairns' formula to waves on a circular core of uniform vorticity, though limited to two dimensions, by working out the excess energy of the Kelvin waves directly from the total kinetic energy of the fluid. The axisymmetric wave ($m = 0$) is omitted. To avoid confusion, we proceed with the real form and set the disturbed core boundary as

$$r = \eta(\theta, t) = 1 + A_0^{(m)} \cos(m\theta - \omega_0 t) \quad (|m| \geqslant 1), \tag{C 1}$$

in place of (3.1).

The solution of the linearized Euler equations for the interior flow field ($r < \eta$) and the velocity potential $\tilde{\phi}_0$ for the exterior irrotational disturbance flow field ($r > \eta$), complying with the boundary conditions, is easily obtained as

$$\left.\begin{aligned} &\tilde{u}_0 = (\omega_0 - m)A_0^{(m)} r^{|m|-1} \sin(m\theta - \omega_0 t), \quad \tilde{v}_0 = \frac{m}{|m|}(\omega_0 - m)A_0^{(m)} r^{|m|-1} \cos(m\theta - \omega_0 t), \\ &\tilde{\phi}_0 = -\frac{\omega_0 - m}{|m|} A_0^{(m)} \frac{1}{r^{|m|}} \sin(m\theta - \omega_0 t). \end{aligned}\right\} \tag{C 2}$$

Alternatively, (C 2) can be obtained as the limit $k_0 \to \infty$ of (3.5) and (3.4) with ω_0 restricted to the isolated branch.

In general, wave energy consists of kinetic and potential energies, and the vortex wave is no exception. It is the centrifugal force that contributes to the potential energy. In the absence of external strain, the basic flow has azimuthal component V_0 only, and when the core is disturbed as (C 1), (2.2) should be taken as

$$\tilde{V}_0 = r \quad \text{for } r < \eta(\theta, t), \qquad \tilde{V}_0 = 1/r \quad \text{for } r > \eta(\theta, t). \tag{C 3}$$

The sensible definition for the kinetic part $K^{(m)}$ of wave energy per unit length in z is provided by gathering together the terms including the disturbance velocity as

$$K^{(m)} = \frac{1}{2}\int_0^{2\pi} \mathrm{d}\theta \left\{ \int_0^{\eta(\theta,t)} \left(2r\tilde{v}_0 + \tilde{u}_0^2 + \tilde{v}_0^2\right) r\,\mathrm{d}r + \int_{\eta(\theta,t)}^{\infty} \left[\frac{2\tilde{v}_0}{r} + \left(\nabla\tilde{\phi}_0\right)^2\right] r\,\mathrm{d}r \right\}. \quad (C\,4)$$

Inserting (C 2) into (C 4) and taking the time average over one period $2\pi/\omega_0$, we are left with, to $O((A_0^{(m)})^2)$,

$$\overline{K^{(m)}} \approx \frac{\pi}{|m|}\left(\omega_0^2 - m^2\right)\left(A_0^{(m)}\right)^2, \quad (C\,5)$$

where the overbar designates the time average. Use of (7.8) further reduces (C 5) to

$$\overline{K^{(m)}} \approx -\pi\left(2 - \frac{1}{|m|}\right)\left(A_0^{(m)}\right)^2. \quad (C\,6)$$

The kinetic part is negative for all $|m| \geqslant 1$. The potential part $U^{(m)}$ of the wave energy per unit length in z is the remaining increment in the total kinetic energy, and is defined by

$$U^{(m)} = \frac{1}{2}\int_0^{2\pi} \mathrm{d}\theta \left\{ \int_0^{\infty} \left(\tilde{V}_0^2 - V_0^2\right) r\,\mathrm{d}r \right\} = \frac{1}{2}\int_0^{2\pi} \mathrm{d}\theta \left\{ \int_1^{\eta(\theta,t)} r^3\,\mathrm{d}r + \int_{\eta(\theta,t)}^{1} \frac{\mathrm{d}r}{r} \right\}. \quad (C\,7)$$

Expanding (C 7) in $A_0^{(m)}$ to quadratic order, we obtain, after taking the time average,

$$\overline{U^{(m)}} \approx \pi\left(A_0^{(m)}\right)^2. \quad (C\,8)$$

The potential energy is positive, implying that the net centrifugal force is effectively restoring. In this way, the total wave energy, the sum of (C 6) and (C 8), restores (7.12).

This coincidence of wave energies calculated via different routes should not be taken for granted. A careful look at (C 4) would lead us to a suspicion that a nonlinear correction, quadratic in $A_0^{(m)}$, to the axisymmetric part of $\tilde{v}_0$, should be taken into account. Conceivably, an infinity of constants of motion in two dimensions, including the conservation of circulation, would preclude the nonlinear axisymmetric component.

In reality, the coincidence does not carry over to three dimensions. If we repeat the same procedure for a general three-dimensional wave, we reach the following form of excess energy:

$$\pi\left\{1 + \frac{2(k_0/\eta_m)^2 K_{|m|}}{k_0 K_{|m|-1} + |m| K_{|m|}}\left[\frac{2(\omega_0 + m)}{\omega_0 - m} + \left(\frac{m(\omega_0 + m)}{2} + k_0^2\right)\frac{K_{|m|}}{k_0 K_{|m|-1} + |m| K_{|m|}}\right]\right\} \times \left(A_0^{(m)}\right)^2, \quad (C\,9)$$

for (k_0, ω_0) satisfying Kelvin's dispersion relation. In the limit $k_0 \to 0$, (C 9), with ω_0 restricted to the isolated branch, coincides with (7.12) and therefore with the long-wave limit of (7.7), but this is not true for $k_0 > 0$. Numerical evidence of § 5 rejects (C 9), since (C 9) would imply that eigenvalue collisions of bending waves ($m = \pm 1$) both with positive energy could drive parametric resonance.

A further support to (7.7) is available from the linear stability analysis of a vortex ring (Fukumoto & Hattori 2003*a*, *b*).

REFERENCES

Abramowitz, M. & Stegun, I. A. 1965 *Handbook of Mathematical Functions*. Dover, New York.

Bayly, B. J. 1986 Three-dimensional instability of elliptical flow. *Phys. Rev. Lett.* **57**, 2160–2163.

Cairns, R. A. 1979 The role of negative energy waves in some instabilities of parallel flows. *J. Fluid Mech.* **92**, 1–14.

Chernous'ko, Yu. L. 1978 An experimental study of secondary multi-eddy flows in elliptical cylinders. *Izv. Atmos. Ocean. Phys.* **14**, 151–153.

Craik, A. D. D. 1985 *Wave Interactions and Fluid Flows*, chap. 2. Cambridge University Press.

Crow, S. C. 1970 Stability theory for a pair of trailing vortices. *AIAA J.* **8**, 2172–2179.

Dellnitz, M., Melbourne, I. & Marsden, J. E. 1992 Generic bifurcation of Hamiltonian vector fields with symmetry. *Nonlinearity* **5**, 979–996.

Eloy, C. & Le Dizès, S. 1999 Three-dimensional instability of Burgers and Lamb–Oseen vortices in a strain field. *J. Fluid Mech.* **378**, 145–166.

Eloy, C. & Le Dizès, S. 2001 Stability of the Rankine vortex in a multipolar strain field. *Phys. Fluids* **13**, 660–676 (referred to herein as EL01).

Eloy, C., Le Gal, P. & Le Dizès, S. 2000 Experimental study of the multipolar vortex instability. *Phys. Rev. Lett.* **85**, 3400–3403.

Friedlander, S. & Vishik, M. M. 1991 Instability criteria for the flow of an inviscid incompressible fluid. *Phys. Rev. Lett.* **66**, 2204–2206.

Fukumoto, Y. & Hattori, Y. 2003*a* Linear stability of a vortex ring revisited. In *Proc. IUTAM Symp. on Tubes, Sheets and Singularities in Fluid Dynamics* (ed. H. K. Moffatt & K. Bajer), pp. 37–48. Kluwer.

Fukumoto, Y. & Hattori, Y. 2003*b* Curvature instability of a vortex ring. *In preparation.*

Gledzer, E. B., Dolzhansky, F. V., Obukhov, A. M. & Ponomarev, V. M. 1975 An experimental and theoretical study of the stability of motion of a liquid in an elliptical cylinder. *Izv. Atmos. Ocean. Phys.* **11**, 617–622.

Gledzer, E. B., Novikov, Yu. V., Obukhov, A. M. & Chusov, M. A. 1974 An investigation of the stability of liquid flows in a three-axis ellipsoid. *Izv. Atmos. Ocean. Phys.* **10**, 69–71.

Gledzer, E. B. & Ponomarev, V. M. 1992 Instability of bounded flows with elliptical streamlines. *J. Fluid Mech.* **240**, 1–30.

Guckenheimer, J. & Mahalov, A. 1992 Instability induced by symmetry reduction. *Phys. Rev. Lett.* **68**, 2257–2260.

Hattori, Y. & Fukumoto, Y. 2003 Short-wavelength stability analysis of thin vortex rings. *Phys. Fluids* (to appear).

Iga, K. 1999 Critical layer instability as a resonance between a non-singular mode and continuous modes. *Fluid Dyn. Res.* **25**, 63–86.

Kerswell, R. R. 2002 Elliptical instability. *Annu. Rev. Fluid Mech.* **34**, 83–113.

Kopiev, V. F. & Chernyshev, S. A. 1997 Vortex ring eigen-oscillations as a source of sound. *J. Fluid Mech.* **341**, 19–57.

Kop'ev, V. F. & Chernyshev, S. A. 2000 Vortex ring oscillations, the development of turbulence in vortex rings and generation of sound. *Phys. Uspekhi* **43**, 663–690.

Krein, M. G. 1950 A generalization of several investigations of A. M. Liapunov on linear differential equations with periodic coefficients. *Dokl. Akad. Nauk. SSSR* **73**, 445–448.

Leweke, T. & Williamson, C. H. K. 1998 Cooperative elliptic instability of a vortex pair. *J. Fluid Mech.* **360**, 85–119.

Lifschitz, A. & Hameiri, E. 1991 Local stability conditions in fluid dynamics. *Phys. Fluids* A **3**, 2644–2651.

MacKay, R. S. 1986 Stability of equilibria of Hamiltonian systems. In *Nonlinear Phenomena and Chaos* (ed. S. Sarkar), pp. 254–270. Adam Hilger, Bristol.

Malkus, W. V. R. 1989 An experimental study of global instabilities due to the tidal (elliptical) distortion of a rotating elastic cylinder. *Geophys. Astrophys. Fluid Dyn.* **48**, 123–134.

Malkus, W. V. R. & Waleffe, F. 1991 Transition from order to disorder in elliptical flow: a direct path to shear flow turbulence. In *Advances in Turbulence III* (ed. A. V. Johansson & P. H. Alfredsson), pp. 197–203. Springer.

Marsden, J. E. 1992 *Lecture on Mechanics*, London Mathematical Society Lecture Note Series, Vol. 174, chap. 10. Cambridge University Press.

Miyazaki, T., Imai, T. & Fukumoto, Y. 1995 Three-dimensional instability of Kirchhoff's elliptic vortex. *Phys. Fluids* **7**, 195–202.

Moore, D. W. & Saffman, P. G. 1971 Structure of a line vortex in an imposed strain. In *Aircraft Wake Turbulence and its Detection* (ed. J. H. Olsen, A. Goldburg & M. Rogers), pp. 339–354. Plenum.

Moore, D. W. & Saffman, P. G. 1975 The instability of a straight vortex filament in a strain field. *Proc. R. Soc. Lond.* A **346**, 413–425 (referred to herein as MS75).

Pierrehumbert, R. T. 1986 Universal short-wave instability of two-dimensional eddies in an inviscid fluid. *Phys. Rev. Lett.* **57**, 2157–2159.

Robinson, A. C. & Saffman, P. G. 1984 Three-dimensional stability of an elliptic vortex in a straining field. *J. Fluid Mech.* **142**, 451–466.

Saffman, P. G. 1988 The stability of vortex arrays to two- and three-dimensional disturbances. *Fluid Dyn. Res.* **3**, 13–21.

Saffman, P. G. 1992 *Vortex Dynamics*, chap. 12. Cambridge University Press.

Tsai, C.-Y. & Widnall, S. E. 1976 The stability of short waves on a straight vortex filament in a weak externally imposed strain field. *J. Fluid Mech.* **73**, 721–733 (referred to herein as TW76).

Vladimirov, V. A., Tarasov, V. F. & Rybak, L. Ya. 1983 Stability of elliptically deformed rotation of an ideal incompressible fluid in a Coriolis force field. *Izv. Atmos. Ocean. Phys.* **19**, 437–442.

Waleffe, F. 1989 The 3D instability of a strained vortex and its relation to turbulence. PhD thesis, Massachusetts Institute of Technology.

Waleffe, F. 1990 On the three-dimensional instability of strained vortices. *Phys. Fluids* A **2**, 76–80.

Widnall, S. E., Bliss, D. B. & Tsai, C.-Y. 1974 The instability of short waves on a vortex ring. *J. Fluid Mech.* **66**, 35–47.

Widnall, S. E. & Tsai, C.-Y. 1977 The instability of the thin vortex ring of constant vorticity. *Phil. Trans. R. Soc. Lond.* A **287**, 273–305.

Yoshida, Z. & Tatsuno, T. 2003 Non-Hermitian spectral theory for the surface-wave model of Kelvin–Helmholtz instability. Preprint.